Title: Hmx3a does not require its homeodomain for its essential functions in spinal cord, ear and lateral line development.

Authors:

Samantha J. England[1], Gustavo A. Cerda[2], Angelica Kowalchuk[1], Taylor Sorice[1], Ginny Grieb[1] and Katharine E. Lewis[1§]

[1]Department of Biology, Syracuse University, 107 College Place, Syracuse, NY 13244, USA

[2]Department of Physiology, Development and Neuroscience, University of Cambridge, Downing Street, Cambridge CB2 3DY, UK.

[§]Corresponding author. Department of Biology, Syracuse University, 107 College Place, Syracuse, NY 13244, USA.

Telephone: +1 315 443 5902; Email: kelewi02@syr.edu

Running Title: Hmx2 and Hmx3 functions in zebrafish development

Abstract

Homeodomain-containing transcription factors have crucial functions in most aspects of cellular function and embryonic development in both animals and plants. Hmx proteins are a sub-family of NK homeodomain proteins and previous research has shown that they have crucial functions in the development of sensory structures such as the eye and the ear. However, the functions of Hmx proteins in spinal cord development have not been analyzed. Here we show that zebrafish *hmx2* and *hmx3a* are co-expressed in spinal dI2 and V1 neurons, whereas *hmx3b*, *hmx1* and *hmx4* are not expressed in the spinal cord. Using mutational analyses, we demonstrate that, in addition to its previously demonstrated role in ear development, Hmx3a is required for survival to adulthood, lateral line progression and correct specification of spinal interneuron neurotransmitter fates. However, despite the fact that *hmx2* and *hmx3a* have similar expression patterns during embryonic development, we have not detected any requirement for Hmx2 in these developmental processes, even when almost all of the *hmx2* locus is deleted. We have also not detected any redundancy between *hmx2* and *hmx3a*: double mutants have identical phenotypes to *hmx3a* single mutants. Even more surprisingly, we have found that Hmx3a does not require its homeodomain for its roles in viability or embryonic development. This is, to our knowledge, the first time that such a prototypical homeodomain protein has been shown not to require its homeodomain.

Introduction

Homeobox-containing genes and the Homeodomain-containing transcription factors that they encode, have crucial functions in most aspects of cellular function and embryonic development in both animals and plants (Burglin and Affolter, 2016). They were also some of the first examples discovered of invertebrate developmental genes that are highly conserved in vertebrates (Carrasco et al., 1984; Gehring, 1985). One important subclass of homeodomain proteins are NK proteins. NK genes are evolutionarily ancient and are an important part of the ANTP megacluster, which also includes Hox and ParaHox genes. NK proteins have crucial roles in the development of mesoderm, endoderm, the nervous system and the heart in all bilaterian animals examined so far (Holland, 2013; Treffkorn et al., 2018; Wotton et al., 2010) and they are also found in sponges, one of the most basal animals still alive, and potentially the sister group to all other animals (Fortunato et al., 2014; Larroux et al., 2007; Pisani et al., 2015; Simion et al., 2017).

Hmx proteins (also called Nk-5 or Nkx-5 proteins, see Table 1) are a key sub-family of NK proteins. In vertebrates there are usually three or four different *Hmx* genes as *Hmx4* is only found in some species (Wotton et al., 2010). Interestingly, *Hmx2* and *Hmx3* are usually located adjacent to each other on the same chromosome and this is also the case for *Hmx1* and *Hmx4*, suggesting that both pairs of genes arose from tandem duplication events rather than the two rounds of whole genome duplication that occurred at the base of the vertebrates (Wotton et al., 2010). In teleosts, there are occasionally extra duplicates of one or more of these genes as the result of the additional genome duplication at the base of the teleosts, although interestingly, the retained genes are not consistent between different teleost species (Wotton et al., 2010). In zebrafish there are two *hmx3* genes, *hmx3a* and *hmx3b,* but only one *hmx1*, *hmx2* and *hmx4* gene.

Previous research has shown that Hmx2 and Hmx3 have crucial functions in ear development in mouse and our recent work shows that this is also the case for Hmx3a in zebrafish (Hartwell et al., 2019; Wang et al., 2001; Wang et al., 2004; Wang and Lufkin, 2005; Wang et al., 1998; see also Feng and Xu, 2010). These genes are also required for correct specification of the mouse hypothalmus (Wang et al., 2004) and morpholino knock-down experiments have suggested that they are required for correct progression of the lateral line in zebrafish (Feng and Xu, 2010). *Hmx2* and *Hmx3* are also expressed in two distinct domains in mouse spinal cord but the identity of these cell types and the functions of Hmx2 and Hmx3 in these cells are unknown (Bober et al., 1994; Wang et al., 2004; Wang et al., 2000).

Here we show that zebrafish *hmx2* and *hmx3a* are co-expressed in spinal dI2 and V1 neurons, whereas *hmx3b*, *hmx1* and *hmx4* are not expressed in the spinal cord. Using mutational analyses, we demonstrate that, in addition to its role in ear development, Hmx3a is required for viability (survival to adulthood), lateral line progression and correct specification of spinal interneuron neurotransmitter fates. However, despite the fact that *hmx2* and *hmx3a* have similar expression patterns during embryonic development, we have not uncovered any requirement for

Hmx2 in viability, or otolith, lateral line or specification of spinal interneuron neurotransmitter fates, even when almost all of the *hmx2* locus is deleted (in our most severe mutant allele, *hmx2*^{SU39}, only 84 nucleotides of 5' sequence and 57 nucleotides of 3' coding sequence remain). We have also not detected any redundancy between *hmx2* and *hmx3a*: *hmx2;hmx3a* double mutants have identical phenotypes to severe *hmx3a* single mutants. Even more surprisingly, we have found that Hmx3a does not require its homeodomain for its roles in viability or embryonic development. This is, to our knowledge, the first time that such a prototypical homeodomain protein has been shown not to require its homeodomain.

Results

hmx2 and *hmx3a* are the only *hmx* genes expressed in spinal cord.

While the expression and functions of zebrafish *hmx* genes have been analyzed in sensory structures such as the eye and the ear, the expression of *hmx1*, *hmx2*, *hmx3a* and *hmx4* in the developing spinal cord has not been investigated and no expression data has previously been reported for *hmx3b*. Therefore, to determine which of the *hmx* genes are expressed in the spinal cord we performed *in situ* hybridizations for *hmx1*, *hmx2*, *hmx3a*, *hmx3b* and *hmx4* at 19 h, 27 h, 36 h, 42 h and 48 h (Fig. 1). At all of these stages, we observed no spinal cord expression of *hmx1*, *hmx3b* or *hmx4* (Fig. 1). However, consistent with previous reports, both *hmx1* and *hmx4* were expressed in the developing eye and ear (Fig. 1; Boisset and Schorderet, 2012; Feng and Xu, 2010; French et al., 2007; Gongal et al., 2011; Marcelli et al., 2014). In contrast, the only expression of *hmx3b* that we observed was weak hindbrain expression at later stages (36-48 h; Fig. 1N', S' & X').

In contrast to *hmx1*, *hmx3b* and *hmx4*, *hmx2* and *hmx3a* are expressed in the spinal cord at all of the stages that we examined (Fig. 1). The spinal cord expression patterns of these two genes are very similar, with the exception that initially, *hmx2* expression appears to be weaker than *hmx3a* and it does not extend as far caudally. Consistent with previous reports, both of these genes are also expressed in the lateral line and developing ear (Fig. 1; Adamska et al., 2000; Feng and Xu, 2010; Hartwell et al., 2019) as well as distinct regions of the brain (data not shown).

As *hmx3a* is expressed in the spinal cord, and teleost duplicate genes often have similar expression patterns, we wanted to further confirm that there was no spinal cord expression of *hmx3b*. Therefore, we performed *in situ* hybridization on *mindbomb (mib)* mutants at 24 h. *mib* encodes an E3-ubiquitin-ligase required for efficient Notch signaling and in mutants for this gene Notch signaling is lost and, as a result, most spinal progenitor cells precociously differentiate into early-forming classes of spinal neurons at the expense of later-forming classes of neurons and glia (Batista et al., 2008; Itoh et al., 2003; Jiang et al., 1996; Park and Appel, 2003; Schier et al., 1996). As a result, weak expression in spinal neurons is often expanded and stronger and hence easier to observe in *mib* mutants at 24 h (Batista et al., 2008; England et al., 2017). However, even in these experiments we saw no expression of *hmx3b* (Fig 1D').

hmx2 and *hmx3a* are expressed in V1 and dI2 interneurons in the spinal cord.

To identify the spinal cord neurons that express *hmx2* and *hmx3a* we performed several different double-labelling experiments. Double *in situ* hybridization with *hmx2* and *hmx3a* confirmed that these genes are co-expressed in the exact same cells in the spinal cord (Fig. 2C). Approximately half of these *hmx2* and *hmx3a (hmx2/3a)* co-expressing spinal cells also co-express *slc32a1* which is only expressed by inhibitory (glycinergic and GABAergic) interneurons and approximately half express *slc17a6a/b* which are only expressed by excitatory (glutamatergic) interneurons (Fig. 2 D & F; see materials and methods for a fuller description of probes used). In

addition, the inhibitory *hmx2/3a*-expressing cells are generally more ventral than the excitatory double-labelled cells. Our previous expression-profiling of V1 interneurons, suggested that these neurons might be the inhibitory cells that express *hmx3a* (Fig. 2B, for a description of these experiments see (Cerda et al., 2009)). Results from our lab and others, have established that the only spinal cord cells that express *engrailed1b* (*en1b*) are V1 interneurons (Batista and Lewis, 2008; Higashijima et al., 2004a). Therefore, to confirm that V1 interneurons also express *hmx3a* we performed double *in situ* hybridizations for *hmx3a* and *en1b*. These experiments showed that all of the *en1b*-expressing spinal cells co-express *hmx3a,* and that approximately half of the *hmx2/3a*-expressing spinal cells co-express *en1b* (Fig. 2E). Taken together, these data clearly identify the inhibitory *hmx2/3a*-expressing spinal cells as V1 interneurons.

As mentioned above, the glutamatergic *hmx2/3a*-expressing cells are generally located dorsal to the inhibitory *hmx2/3a*-expressing cells. Therefore, these excitatory cells could be V0v, dI5, dI3, dI2 or dI1 interneurons (Fig. 2a; Cheng et al., 2005; Grossmann et al., 2010; Satou et al., 2012; Talpalar et al., 2013). We performed double labelling experiments with markers of different cell types and found that all *hmx2/3a*-expressing spinal cells co-express *lhx1a* and *lhx5* (Fig. 2B & G). Lhx1a and Lhx5 are predominantly expressed by inhibitory spinal cord interneurons, but they are also expressed by dI2 interneurons, which are excitatory (Alaynick et al., 2011; Cheng et al., 2004; Gowan et al., 2001; Gross et al., 2002; Moran-Rivard et al., 2001; Muller et al., 2005; Muller et al., 2002; Satou et al., 2012; Wine-Lee et al., 2004). The only other excitatory neurons that might express these two *Lhx* genes are V0v interneurons. Recent single-cell RNA-Seq (scRNA-Seq) data from mouse identified V0 cells that express *lhx1a* and *lhx5*, although it is not clear whether these cells were excitatory V0v and/or inhibitory $V0_D$ cells (Delile et al., 2019). As V0v cells are the only spinal cord cells that express *evx1* and *evx2* (Juárez-Morales et al., 2016 and references therein), we tested whether there was any co-expression of *hmx3a* and *evx1/2* using double *in situ* hybridization as well as immunohistochemistry for GFP and *in situ* hybridization for *hmx3a* in Tg(*evx1:EGFP*)^{SU1} and Tg(*evx1:EGFP*)^{SU2} embryos. However, we did not observe any co-expression in any of these experiments (Fig. 2H and data not shown). Therefore, we are confident that the excitatory *hmx2/3a*-expressing spinal cells are dI2 interneurons. Consistent with this, recent mouse scRNA-Seq data suggests that mouse *Hmx2* and *Hmx3* are also expressed in V1 and d2 spinal interneurons (Delile et al., 2019).

<u>Morpholino knock-down experiments suggest that Hmx2 and Hmx3a may be redundantly required for correct specification of spinal cord interneuron glutamatergic phenotypes.</u>

As an initial step to try and identify the function(s) of Hmx2 and Hmx3a in spinal cord development we performed morpholino knock-down experiments. As previous analyses suggested that these genes have redundant roles in ear and lateral line development (Feng and Xu, 2010), we designed and injected morpholinos for each of the genes separately and in combination (see materials and methods). Consistent with this previous report, we observed fused otoliths and stalled lateral line progression in embryos co-injected with the two morpholinos (Feng and Xu, 2010; data not shown). When we analyzed spinal cord phenotypes in double morpholino knock-down (DKD)

embryos, we saw no change in the number of *hmx3a*- or *en1b*-expressing cells, suggesting that dI2 and V1 interneurons still form in normal numbers (Fig. 3A-F). However, when we examined markers of neurotransmitter fates we observed a reduction in the number of spinal excitatory (glutamatergic) cells and a corresponding increase in inhibitory cells, suggesting that at least some dI2 neurons had switched their neurotransmitter phenotype from glutamatergic to inhibitory (Fig. 3G-L). Our analyses of single knock-down (SKD) embryos suggested that *hmx2* and *hmx3a* might act partially redundantly in this process as we observed less severe reductions in the number of spinal glutamatergic cells in these embryos (Fig. 2I). To confirm the specificity of these knock-down results, we tested whether co-injecting a morpholino resistant *hmx3a* RNA with the *hmx2* and *hmx3a* morpholinos could rescue the spinal cord phenotype of DKD embryos and we were able to obtain a partial rescue in the number of glutamatergic neurons (Fig. 3M-O and Table 2). Injections of higher amounts of RNA led to considerable embryo death, probably because of the toxic effects of injecting considerable amounts of both RNA and morpholinos into the embryos.

Mutational analyses demonstrate that Hmx2 is not required, and that Hmx3a does not require its DNA-binding homeodomain, for viability or correct development of lateral line, ear or spinal interneurons.

To further test the hypothesis that *hmx2* and *hmx3a* are required for the correct specification of spinal interneuron neurotransmitter fates we created CRISPR mutants in each of these genes, targeting the same region upstream of the homeodomain (see materials and methods). We also obtained a $hmx3a^{sa23045}$ allele from the sanger zebrafish mutation project (Kettleborough et al., 2013) that has a stop codon upstream of the homeodomain.

As our morpholino-injected embryos had fused otoliths, and our previous analyses had shown that this was also the case in $hmx3a^{SU3}$ mutants (Hartwell et al., 2019), we expected that *hmx2* mutants would have this same phenotype. However, we did not detect any otolith fusion phenotypes in embryos homozygous for four different *hmx2* alleles ($hmx2^{SU35}$, $hmx2^{SU36}$, $hmx2^{SU37}$, $hmx2^{SU38}$; Fig. 4, data not shown). In addition, all four of these mutant alleles are homozygous viable (Fig. 4, Table 3). We also examined lateral line progression and the number of spinal cord glutamatergic neurons in $hmx2^{SU37}$ and $hmx2^{SU38}$ homozygous mutants and did not detect any change compared to WT embryos (Table 2 and data not shown).

Surprisingly, embryos homozygous for $hmx3a^{SU42}$ also do not have fused otoliths or stalled lateral line progression (Fig. 4, Fig. 5C & I). They also have normal numbers of spinal cord glutamatergic neurons and are homozygous viable (Fig. 4, Fig 5 O & T, Tables 2 & 3). Interestingly, embryos homozygous for $hmx3a^{sa23054}$ have variable, incompletely penetrant otolith fusion phenotypes that range from no fusion, through incomplete fusion (Fig. 5D), to complete fusion, despite the fact that any protein encoded by this allele should retain more WT sequence than that encoded by $hmx3a^{SU42}$ (Fig 4). However, $hmx3a^{sa23054}$ mutants have normal lateral line progression, no reduction in the number of spinal cord glutamatergic neurons and they are also viable (Fig. 4, Fig. 5 J, P & U, Tables 2 & 3).

In contrast, embryos homozygous for *hmx3a*^{SU3} or *hmx3a*^{SU43} have a fully penetrant fused otolith phenotype, stalled lateral line progression and are homozygous lethal (Fig. 4, Fig. 5E, K, Table 3, also see (Hartwell et al., 2019) for a detailed description of the *hmx3a*^{SU3} ear phenotype). When we examined the spinal cords of embryos homozygous for these mutant alleles, we observed a statistically significant reduction in the number of glutamatergic cells, but in each case the change was smaller than we had previously observed for morpholino-injected DKD embryos (Fig. 5Q & V, Table 2). We also examined the expression of *slc32a1* in *hmx3a*^{SU3} mutants and found that there was an increase in the number of inhibitory spinal interneurons, although, again, the increase was less than in the DKD morpholino-injected embryos (Fig. 6C, H, M, Table 2). However, similar to the DKD embryos there was no change in the number of spinal *hmx3a*- or *en1b*-expressing cells in *hmx3a*^{SU3} mutants, suggesting that dI2 and V1 interneurons are forming in normal numbers and not dying or changing into different classes of interneurons (Fig. 6A, B, F, G, K, L, Table 2).

To test whether our *hmx2* mutants had no obvious phenotypes because they had retained some Hmx2 function, we created a deletion allele, *hmx2*^{SU39}, in which almost all of the *hmx2* genomic sequence is deleted. Only 84 nucleotides of 5' sequence and 57 nucleotides of very 3' coding sequence remain (Fig. 4). However, *hmx2*^{SU39} homozygous mutants also lack fused otoliths, have normal lateral line progression and are homozygous viable (Fig. 4, Fig 5 B & H, Tables 2 & 3). In addition, there is no change in the number of glutamatergic cells in the spinal cords of these mutants, when compared to WT sibling embryos (Fig. 5 N & S, Table 2).

While this was surprising, we hypothesized that Hmx3a was acting redundantly with Hmx2 and could compensate for its loss. To test this hypothesis, we created double mutant alleles. As *hmx2* and *hmx3a* are adjacent on the same chromosome, and our single mutant analyses suggested that even severely truncated Hmx2 and/or Hmx3a proteins might retain some function, we reasoned that the clearest way to test this hypothesis was to delete as much of the *hmx2/hmx3a* genomic region as possible. We created two different mutant alleles, *hmx2;hmx3a*^{SU44} and *hmx2;hmx3a*^{SU45}, that differ only in the amount of remaining upstream sequence. In both of these alleles the entire *hmx3a* coding and all but the last 66 nucleotides of *hmx2* coding sequence are deleted (Fig. 4 and materials and methods). However, in double mutant embryos homozygous for these large deletion alleles, the reduction in the number of excitatory spinal interneurons is equivalent to that in *hmx3a*^{SU3} or *hmx3a*^{SU43} single mutants (Fig. 5V & W and Table 2). We also see no obvious differences in the otolith fusion or lateral line progression phenotype between these single and double mutants (Fig. 5 E, F, K and L).

To determine whether the increase in the number of spinal inhibitory interneurons reflects an increase in glycinergic or GABAergic neurons, we examined the expression of genes expressed exclusively by cells with these neurotransmitter phenotypes (see materials and methods) in double mutants. While we found no statistically significant difference in the number of spinal cord glycinergic cells in *hmx2;hmx3*^{SU44} mutants, there was a

statistically significant increase in the number of GABAergic cells in these mutants compared to WT sibling embryos (Fig. 6D, E, I, K, N, O, Table 2).

As *hmx2* expression is initially weaker than *hmx3a* expression, we also analyzed *hmx2*^{SU39} single mutants at 48 h, to determine if there was a spinal cord neurotransmitter phenotype at this later stage of development. We examined the number of GABAergic cells, as these are easier than glutamatergic cells to count at this stage. However, there was no change in the number of GABAergic spinal cells in *hmx2*^{SU39} single mutants compared to WT embryos (Table 2). We also tested whether the spinal phenotype of double mutants was more severe than *hmx3a*^{SU3} single mutants at 48 h. However, while the number of GABAergic cells was increased in both *hmx3a*^{SU3} single mutants and *hmx2;hmx3a*^{SU44} double mutants, there was no statistically significant difference between these two phenotypes (Fig. 6P, Q, S, T, V & W, Table 2). Taken together, these results suggest that Hmx2 is not required for viability, lateral line progression, or correct development of ear otoliths or spinal interneuron neurotransmitter phenotypes. Our data also suggest that while Hmx3a is required for viability, lateral line progression, and correct development of ear otoliths and spinal interneuron neurotransmitter phenotypes, it does not require its homeodomain for its essential functions in these aspects of development.

<u>Trans heterozygous crosses suggest that our *hmx3a* mutations form an allelic series</u>

hmx3a^{SU3}, *hmx3a*^{SU42} and *hmx3a*^{SU43} mutant alleles all introduce a frameshift within 4 nucleotides of each other (nucleotide 319, 320, and 323 of the coding sequence respectively). Assuming that all three of these alleles are translated into truncated proteins, *hmx3a*^{SU3} would retain 106 WT amino acids whereas the other two alleles would retain 107 WT amino acids (Fig. 4). However, despite the similarity of these mutant alleles, embryos homozygous for *hmx3a*^{SU3} and *hmx3a*^{SU43} have fused otoliths, stalled lateral line progression, a reduction in the number of spinal excitatory interneurons and do not survive to adulthood whereas embryos homozygous for *hmx3a*^{SU42} are viable and lack these developmental phenotypes. In addition, as mentioned above, *hmx3a*^{sa23054} mutants have variable otolith fusion phenotypes, despite retaining more WT sequence than *hmx3a*^{SU3}, *hmx3a*^{SU42} or *hmx3a*^{SU43} alleles. Therefore, to further analyze the relative "strength" of these *hmx3a* mutant alleles, we made different pair-wise crosses between fish heterozygous for *hmx3a*^{SU3}, *hmx3a*^{SU42}, *hmx3a*^{SU43}, *hmx3a*^{sa23054} and *hmx2;hmx3a*^{SU44} and analyzed both ear and lateral line development in the resulting embryos. As the *hmx2;hmx3a*^{SU44} allele lacks all *hmx3a* coding sequence and only retains the last 66 nucleotides of *hmx2* coding sequence (Fig. 4) we assume that this is a deletion of both genes when interpreting the results of these trans-het analyses.

Interestingly, when we crossed fish heterozygous for *hmx2;hmx3a*^{SU44} with fish heterozygous for *hmx2*^{SU39} the resulting embryos had normal otolith development and lateral line progression (Table 4). Given that approximately a quarter of these embryos should lack both alleles of *hmx2* and one allele of *hmx3a*, this demonstrates that one WT allele of *hmx3a* is sufficient for normal otolith development and lateral line progression.

As expected, as both alleles produce homozygous mutant phenotypes, when we crossed fish heterozygous for *hmx3a*^{SU3} with fish heterozygous for *hmx3a*^{SU43} we observed mendelian ratios of embryos with fused otoliths and stalled lateral line progression phenotypes identical to those of the homozygous mutants (Table 4). Similarly, we obtained mendelian ratios of embryos with fused otoliths and stalled lateral line progression when we crossed fish heterozygous for *hmx3a*^{SU3} with fish heterozygous for *hmx2;hmx3a*^{SU44}, or fish heterozygous for *hmx3a*^{SU43} with fish heterozygous for *hmx2;hmx3a*^{SU44}. Interestingly though, in the latter cross, a small number of embryos with stalled lateral line progression had a weaker phenotype, where the lateral line primordium migrated slightly more caudally than is the case in *hmx3a*^{SU3}, *hmx3a*^{SU43} or *hmx2;hmx3a*^{SU44} homozygous mutants (Table 4, weaker phenotype was similar to Fig. 6U).

Even more interestingly, when we crossed fish heterozygous for *hmx3a*^{sa23054} with fish heterozygous for either *hmx2;hmx3a*^{SU44} or *hmx3a*^{SU3} we also obtained mendelian ratios of embryos with fully penetrant otolith fusion phenotypes and stalled lateral line progression (although some embryos had the slightly weaker lateral line phenotype described above), as opposed to the variable otolith fusion phenotypes and normal lateral line progression that occurs in *hmx3a*^{sa23054} homozygous mutants (Table 4). This suggests that while two *hmx3a*^{sa23054} alleles are sufficient for normal lateral line progression and also sometimes normal otolith development, this is not the case for either one *hmx3a*^{sa23054} allele or the combination of *hmx3a*^{sa23054} and *hmx3a*^{SU3} alleles.

More surprisingly, when we crossed fish heterozygous for *hmx3a*^{SU42} with fish heterozygous for either *hmx2;hmx3a*^{SU44} or *hmx3a*^{SU3} we also obtained embryos with fused otoliths and stalled lateral line progression (although most embryos had the slightly weaker lateral line phenotype, Fig. 6D, Table 4). For the combination of *hmx3a*^{SU42} and *hmx2;hmx3a*^{SU44} these phenotypes occurred in mendelian ratios. However, for the combination of *hmx3a*^{SU3} and *hmx3a*^{SU42}, while we observed a mendelian ratio of embryos with stalled lateral line progression, the percentage of embryos with fused otoliths was less than 13%.

Taken together with our analyses of homozygous mutants, these results suggest that these different mutant alleles comprise an allelic series in which *hmx2;hmx3a*^{SU44} is the most severe loss-of-function allele, followed by *hmx3a*^{SU3}, *hmx3a*^{SU43}, *hmx3a*^{sa2305} and *hmx3a*$^{SU42.}$ As our previous results comparing double mutants to *hmx3a* single mutants suggest that *hmx2* is not required or sufficient for correct ear or lateral line development, it is likely that the *hmx2;hmx3a*^{SU44} allele is more severe than *hmx3a*^{SU43} and *hmx3a*^{SU3} because more of the *hmx3a* locus is deleted and not because *hmx2* is also missing. This, in turn, suggests that all of the other *hmx3a* alleles, including *hmx3a*^{SU3}, are hypomorphs, although they have different levels of retained function. At the other end of the allelic series, while two alleles of *hmx3a*^{SU42} are sufficient for normal otolith development and lateral line progression, one allele is not. As one WT allele of *hmx3a* is sufficient for normal development, these results suggest that *hmx3a*^{SU42} is a hypomorphic allele.

The lack of a *hmx2* mutant phenotype and the incompletely penetrant spinal cord phenotype in *hmx3a* mutants is not due to maternal expression of *hmx* genes.

One possible explanation for why the spinal cord phenotype is less severe in *hmx2/3a* double mutants than morpholino-injected DKD embryos would be if *hmx2* and/or *hmx3a* are maternally expressed, as in this case the morpholinos might knock-down both maternal and zygotic function whereas the mutants would only remove zygotic function. To test this, we performed *in situ* hybridization for *hmx2* and *hmx3a* at the 16-cell stage. However, we did not detect any maternal expression of *hmx2*, *hmx3a* or any of the other *hmx* genes (Fig. 7A-E). We also generated embryos from fish homozygous mutant for $hmx2^{SU38}$, $hmx3a^{SU39}$ and $hmx3a^{sa23054}$. However, even though half of the embryos in each of these crosses should have been maternal zygotic mutants, we did not observe any embryos with fused otoliths (Fig. 4).

The incomplete penetrance of the spinal cord phenotype in *hmx3a* and *hmx2;hmx3a* mutants is not due to upregulation of *hmx3b*, *hmx1* or *hmx4* expression.

Even though *hmx3b*, *hmx1* or *hmx4* are not normally expressed in the spinal cord, it was theoretically possible that they were upregulated in the spinal cord in response to the absence, or reduced levels, of either Hmx2 and/or Hmx3a function. Therefore, to test this, we performed *in situ* hybridization for these genes in $hmx3a^{SU3}$ and $hmx2;hmx3a^{SU44}$ mutants at 27 h. In all cases, we did not observe any expression of these genes in either genotyped mutants or their sibling embryos (data not shown).

$hmx3a^{SU42}$ mutant alleles do not lack a spinal cord phenotype because of genetic compensation

Recent reports have demonstrated that genetic compensation can lead to loss-of-function mutants in a gene having a less severe phenotype than embryos injected with a morpholino against the same gene (El-Brolosy et al., 2019; El-Brolosy and Stainier, 2017; Peng, 2019; Rossi et al., 2015; Sztal et al., 2018; Zhu et al., 2017). It is thought that in these cases, other genes that can compensate for the mutated gene are upregulated in mutant embryos. If this is the case, then morpholino knock-down should have less effect on mutant embryos than on WT sibling embryos, because the morpholino will not affect any upregulated compensating genes (e.g. see Rossi et al., 2015; Sztal et al., 2018). Therefore, to test whether the lack of a spinal cord phenotype in $hmx3a^{SU42}$ mutants was due to genetic compensation, we injected the *hmx3a* morpholino into embryos from a cross of fish heterozygous for $hmx3a^{SU42}$ and performed *in situ* hybridization for *slc17a6* to label glutamatergic (excitatory) spinal interneurons. When we examined the injected embryos down a stereo microscope we were able to separate them into one group that had an obvious reduction in spinal glutamatergic cells and another group that either lacked, or had a more subtle, phenotype. However, when we genotyped these embryos we found similar numbers of homozygous mutant and WT embryos in both groups and the frequencies of different genotypes in each group were not statistically significantly different from Mendelian rations (Table 5). In addition, when we compared the average number of glutamatergic cells in morpholino-injected WT and mutant embryos, there was no statistically significant

difference between them, regardless of whether we compared all of the morpholino-injected embryos of each genotype or just compared embryos within the same phenotype group (Table 5). These data suggest that the lack of an abnormal spinal cord phenotype in *hmx3a*^{SU42} homozygous mutant embryos is not due to genetic compensation and that the differences that we observed between the two groups of injected embryos just reflect exposure to different levels of morpholino (see materials and methods). Consistent with this, we also do not see any nonsense mediated decay (NMD) of *hmx3a* mRNA in *hmx3a*^{SU42} mutants (Fig. 7F; NMD has been suggested to play a key role in at least some instances of genetic compensation (El-Brolosy et al., 2019)).

<u>The incomplete penetrance of the spinal cord phenotype in *hmx3a*^{SU3} mutants is not due to genetic compensation</u>

We also tested whether the spinal cord phenotype of *hmx3a*^{SU3} mutants is less severe than embryos injected with a *hmx3a* morpholino because of genetic compensation. As above, we injected the *hmx3a* morpholino into embryos from a cross of fish heterozygous for *hmx3a*^{SU3} and performed *in situ* hybridization for *slc17a6* to label glutamatergic (excitatory) spinal interneurons. When we examined these embryos down a stereomicroscope, some of the embryos appeared to have a severe reduction in glutamatergic cells that resembled the morpholino knock down phenotype, whereas in the other embryos any reduction was more subtle. However, when we genotyped these embryos we again found similar numbers of homozygous mutant and WT embryos in both groups and the frequencies of the different genotypes in each group were not statistically significantly different from Mendelian rations (Table 6). In addition, when we compared the average number of glutamatergic cells in morpholino-injected WT and mutant embryos, there was no statistically significant difference between them, regardless of whether we compared all of the morpholino-injected embryos, or just compared the injected embryos within a particular phenotype group (Table 6). For the "weaker" phenotype group of injected embryos, the difference between WT and mutant embryos approached statistical significance. However, this is probably because some of the WT embryos in this category had almost no reduction in the number of glutamatergic cells, whereas all of the mutants in this category had at least their normal mutant phenotypes. These results suggest that the differences that we observed between the two groups of injected-embryos probably just reflect exposure to different levels of morpholino (see materials and methods), and that embryos in the "weaker" phenotype group did not receive sufficient morpholino to effectively knock-down *hmx3a* RNA or cause the more severe morpholino phenotype. Taken together, these data suggest that the spinal cord phenotype in *hmx3a*^{SU3} homozygous mutant embryos is not less severe than the morpholino knock-down phenotype because of genetic compensation. Consistent with this, we also do not see any nonsense mediated decay (NMD) of *hmx3a* mRNA in *hmx3a*^{SU3} mutants (Fig. 7H).

Discussion

Zebrafish Hmx2 is not required for correct otolith, lateral line or spinal cord neurotransmitter phenotypes.

The data reported in this paper, suggest two surprising results. The first is that Hmx2 is not required for either viability or correct otolith, lateral line or spinal cord neurotransmitter phenotypes in zebrafish and the second is that Hmx3a does not require its homeodomain for its essential roles in these processes. Both the sequence and the expression of Hmx2 and Hmx3 are highly conserved in different animals (Wotton et al., 2010), and it has even been reported that Drosophila *hmx* can substitute for the loss of *Hmx2* and *Hmx3* in mouse ear development (Wang et al., 2004; Wang and Lufkin, 2005), suggesting that the functional capabilities of Hmx proteins are also highly conserved. Previous analyses demonstrated that mouse *Hmx2* mutants had defects in ear development, although interestingly these were more severe in about 70% of homozygous mutants than in the other 30%, showing that there was some variability in the mutant phenotypes (Wang et al., 2001). In addition, mouse *Hmx2;Hmx3* double mutants had more severe ear phenotypes than either single mutant, as well as defects in hypothalmus and pituitary development that were not found in either single mutant and most of the double mutants died around the 5th day after birth, whereas the single mutants were viable (Wang et al., 2004). Taken together, these data suggest that mouse Hmx2 has important functions in ear and brain development, although some of these are redundant with Hmx3. This is very different to our results in zebrafish where even *hmx2*^{SU39} mutants, that lack almost all coding sequence, are viable and lack any obvious mutant phenotypes and *hmx2;hmx3a* double mutants have the same mutant phenotypes as severe *hmx3a* single mutants. Our experiments suggest that the lack of obvious phenotypes in *hmx2*^{SU39} single mutants is not due to genetic compensation, maternal expression of *hmx* genes or to other *hmx* genes being upregulated in the absence of Hmx2. It is still possible that *hmx2* functions later in development and/or in aspects of development that we did not assay. However, if this is the case, these functions are not required for viability as even *hmx2*^{SU39} homozygous mutants survive to adulthood. It is also possible that *hmx2* has important function(s) in adult fish, as our assays would not have detected this. However, even if this is the case, it is striking that zebrafish *hmx2* is expressed in the developing ear, lateral line and specific spinal cord interneurons, but does not appear to be required for the development of these sensory structures and neurons. It is also unclear why zebrafish *hmx2* cannot substitute at-least-partially for loss of *hmx3a*, when it can in mouse.

Hmx3a does not require its homeodomain for its functions in viability and otolith, lateral line and spinal cord interneuron development and very similar mutant alleles have different phenotypes.

It is also surprising that Hmx3a does not require its homeodomain for either its role in viability or its essential functions in otolith development, lateral line progression and correct specification of spinal cord neurotransmitter phenotypes. As mentioned previously, to our knowledge, this is the first time that such a prototypical homeodomain protein has been shown not to require its homeodomain for normal function.

In addition, we see different phenotypes in *hmx3a* mutant alleles that have very similar amounts of remaining WT coding sequence. Our analyses of homozygous and trans-heterozygous mutants suggest that we have created an allelic series of *hmx3a* mutant alleles in which *hmx2;hmx3a*^{SU44} is the most severe allele, followed by *hmx3a*^{SU3}, *hmx3a*^{SU43}, *hmx3a*^{sa2305} and *hmx3a*^{SU42}. We assume that *hmx2;hmx3a*^{SU44} allele is a complete loss of function for *hmx3a* as the *hmx3a* coding sequence is completely deleted. Our results suggest that *hmx3a*^{SU3} is the next strongest allele, as it is the only allele that only produced strong lateral line phenotypes when in combination with *hmx2;hmx3a*^{SU44}, although there may not be much difference in phenotypic strength between *hmx3a*^{SU3} and *hmx3a*^{SU43}. However, as only 13% of embryos from a cross of *hmx3a*$^{SU42/+}$ and *hmx3a*$^{SU3/+}$ parents have fused otoliths whereas 22% of embryos from a cross of *hmx3a*$^{SU42/+}$ and *hmx2;hmx3a*$^{SU44/+}$ parents do, it is likely that *hmx3a*^{SU3} is a hypomorph rather than a complete loss of function allele. *hmx3a*^{sa2305} retains more WT function than both *hmx3a*^{SU3} and *hmx3a*^{SU43} as *hmx3a*^{sa2305} homozygous mutants only have variable otolith fusion phenotypes and they are also viable and have normal lateral line progression and no change in the number of spinal cord glutamatergic neurons. In contrast, *hmx3a*^{SU42} mutants lack all of these mutant phenotypes. However, even though *hmx3a*^{SU42} homozygous mutants have no obvious mutant phenotypes and are viable, one allele of *hmx3a*^{SU42} is not sufficient for normal otolith development and lateral line progression, even though one WT allele of *hmx3a* is. This suggests that the *hmx3a*^{SU42} allele is also hypomorphic.

It is currently unclear why *hmx3a*^{SU42} retains more WT Hmx3a function than *hmx3a*^{SU43} when both should encode proteins with only 107 WT amino acids. We do not see any NMD of *hmx3a* mRNA for any of these *hmx3a* single mutant alleles (Fig. 7F-I; the double mutant lacks all *hmx3a* coding sequence, so there is no mRNA to assess), so the difference in allelic strength is not due to some of the mutant mRNAs being degraded. However, it is still theoretically possible that the different alleles result in different amounts of truncated protein, due to differences in protein stability. It is also possible that the overall length of the mutant protein is important for retaining function and that the additional abnormal amino acids after the frameshift but before the premature stop codon in *hmx3a*^{SU42} help this allele retain more WT function. If this is the case, then it could also explain why *hmx3a*^{SU42} appears to retain more WT function than *hmx3a*^{sa23054}, which should encode an extra 11 amino acids of WT protein sequence, but is shorter overall.

<u>Hmx3a is required for correct neurotransmitter phenotypes of a subset of spinal interneurons</u>

Our spinal cord analyses have identified, for the first time, a requirement for Hmx3a in spinal interneuron development. We have shown that *hmx2* and *hmx3a* are expressed by V1 and dI2 interneurons, which is consistent with very recent scRNA-Seq data from mouse (Delile et al., 2019). While the respective *in situ* hybridization probes are not strong enough to formally confirm with double-labelling experiments that dI2 interneurons switch their neurotransmitter phenotype from glutamatergic to GABAergic in embryos that lack Hmx3a function, this is the most likely explanation of our data. *hmx3a* is only expressed by dI2 and V1 interneurons in the spinal cord, and of these cell types, only dI2 interneurons are glutamatergic. Therefore, the most likely explanation for the

reduction in the number of glutamatergic spinal cord cells in *hmx3a* mutants and morpholino-injected knock-down embryos is that dI2 neurons are losing their glutamatergic phenotypes. Given that we also see a corresponding increase in GABAergic spinal cord cells, but the number of V1 cells (indicated by *en1b* expression) does not change, it is likely that the dI2 interneurons that are losing their glutamatergic phenotypes are becoming GABAergic instead.

Our original morpholino data suggested that all dI2 interneurons might be switching their neurotransmitter phenotypes as the increase in the number of spinal inhibitory cells and the reduction in the number of excitatory spinal cells in DKD embryos were both roughly equal to the number of dI2 interneurons (glutamatergic *hmx3a*-expressing cells). However, even in our *hmx2;hmx3a* double mutants the number of cells changing their neurotransmitter phenotypes is considerably lower: roughly half as many cells as in the DKD embryos. The differences between morpholino-injected embryos and mutant embryos can be seen most clearly in our experiment to test whether genetic compensation occurrs in *hmx3a*^{SU3} homozygous mutants. These data directly compare uninjected mutants with morpholino-injected mutants and WT siblings from the same experiment. While there were a range of morpholino-injected phenotypes, overall the *hmx3a* morpholino-injected WT and *hmx3a*^{SU3} mutant embryos had a more severe reduction of glutamatergic cells than uninjected mutants (Table 5). While *hmx3a*^{SU3} mutants may be slightly hypomorphic (as discussed above), their spinal cord phenotype is the same as *hmx2;hmx3a*^{SU44} mutants, in which the *hmx3a* coding sequence is completely deleted. Therefore, the more severe phenotypes in some of the *hmx3a*^{SU3} mutants injected with *hmx3a* morpholino cannot be explained by the morpholino removing any residual Hmx3a function. Instead, these data suggest that the less severe phenotype in uninjected *hmx3a*^{SU3} and *hmx2;hmx3a*^{SU44} mutants is not caused by genetic compensation. We have also shown that this less severe phenotype is not due to maternal expression of *hmx* genes or to other *hmx* genes being upregulated in these mutants. Combined with the fact that the *hmx2* morpholino-injected SKD embryos have reduced numbers of spinal glutamatergic cells, while *hmx2*^{SU39} mutants do not, this suggests that both the *hmx3a* and *hmx2* morpholinos may have non-specific effects on neurotransmitter phenotypes in the spinal cord. Consistent with this, there is also a body curvature phenotype in the morpholino-injected embryos that is not present in the mutants. Our data suggest that the *hmx3a* morpholino also has specific effects, as we were able to partially rescue the DKD embryo phenotype by co-injecting a morpholino-resistant *hmx3a* mRNA. Interestingly, we rescued about 19 glutamatergic cells in these experiments, which is roughly equivalent to the number of cells that lose their glutamatergic phenotypes and/or gain inhibitory phenotypes in *hmx3a*^{SU3} and *hmx2;hmx3a*^{SU44} mutants at the same stage, suggesting that we may have rescued all of the specific effects of the *hmx3a* morpholino.

One puzzling thing, however, about this interpretation of the data is that the morpholino knock-down phenotypes appeared to be specific. Our experiments suggested that the reduction in glutamatergic cells in DKD embryos was unlikely to be due to cell death or a delay in embryo development as there was no change in the number of *hmx3a*- or *en1b*-expressing spinal cord cells in these embryos and there was an increase in the number of inhibitory spinal

interneurons equivalent to the reduction in glutamatergic neurons. This is surprising, as it suggests that if the more severe DKD phenotype is due to non-specific effects of the morpholinos, this non-specific effect produces an identical phenotype to the specific knock-down effect, namely a switch in neurotransmitter fate. It is also surprising, given our mutant analyses, that the *hmx2* morpholino has the same effect as the *hmx3a* morpholino. The two morpholino sequences are completely different from each other and there is no homology between the *hmx2* morpholino and *hmx3a* upstream or coding sequence. When we blast the *hmx2* morpholino sequence against the zebrafish genome the only homology is with *hmx2* (25/25 residues) and with intron sequence for a gene *si:dkey-73p2.3* on chromosome 3 (18/25 residues) which is predicted to encode a protein with GTP-binding. Similarly, when we blast the *hmx3a* morpholino sequence against the zebrafish genome the only homology is with *hmx3a* (25/25 residues).

One intriguing alternative possibility that could explain the apparent specificity of the additional phenotype in the morpholino-injected embryos could be that Hmx3a is acting as a fate guarantor, to make the normal neurotransmitter phenotype more robust, as has previously been described for some transcription factors (Topalidou et al., 2011; Zheng and Chalfie, 2016; Zheng et al., 2015). In these cases, mutating the gene usually caused a partially penetrant phenotype in ideal conditions but a more severe phenotype in stressed conditions. In this case, the injection of morpholinos could be such a stressed condition, and this could account for the more severe phenotype. Future analyses could investigate this possibility by testing if other stressed conditions increase the severity of *hmx3a*^{SU3} single mutant or *hmx2;hmx3a* double mutant phenotypes.

<u>*hmx3b* has very limited expression during early zebrafish embryogenesis.</u>

The data in this paper also provide the first characterization of zebrafish *hmx3b* expression. Surprisingly, given the expression of all of the other four *hmx* genes during zebrafish embryonic development we have only been able to detect very weak expression of *hmx3b* in the hindbrain from 36-48 h (Fig. 1 N', S' & X'). When we performed our earlier analyses of vertebrate NK genes, we did not find *hmx3b* in either the Zv7 or Zv8 versions of the zebrafish genome (Wotton et al., 2010). It did not appear until Zv9. Interestingly, despite *Hmx2* and *Hmx3* being closely linked in all vertebrates examined so far, only one *hmx2* gene has been found in the zebrafish genome and zebrafish *hmx3b* is not located within any of the previously described duplicated NK homeobox clusters, including the teleost duplications: it is located on chromosome 12, separate from any other Nk genes (Wotton et al., 2010). However, *hmx3b* is flanked by two genes, *bub3* and *acadsb*, that flank *Hmx2* and *Hmx3* in the human, mouse, chicken and xenopus genomes, suggesting that part of the NK cluster previously identified on chromosome 1 may have translocated to chromosome 12. This is maybe not surprising as zebrafish *hmx2* and *hmx3a* have also translocated from the rest of their NK cluster on Chromosome 13 to Chromosome 17 and zebrafish *hmx1* and *hmx4* have translocated from the rest of their cluster on chromosome 14 to chromosome 1 (Wotton et al., 2010). It is possible that this translocation and the loss of surrounding sequences may explain the different expression pattern of *hmx3b* compared to *hmx3a*. For example, there is a highly conserved non-coding region located between

hmx2 and *hmx3a* that is conserved in mammals, frog and teleosts (Wotton et al., 2010) but this region is not present near *hmx3b* (data not shown).

Conclusions

In conclusion, in this paper we provide the first description of zebrafish *hmx3b* expression. Our results also identify the spinal cord cells that express *hmx2* and *hmx3a* (dI2 and V1 interneurons) and uncover a novel function for Hmx3a in correct specification of spinal neurotransmitter phenotypes. Our data suggest that while Hmx3a is required for viability, correct otolith development, lateral line progression and specification of spinal neurotransmitter phenotypes, Hmx2 is not required for any of these developmental processes. Finally our results also suggest that Hmx3a does not require its homeodomain for its roles in viability or embryonic development. Taken together, these findings significantly enhance our understanding of spinal cord, ear and lateral line development and suggest that homeobox proteins may not require their homeobox domain for their normal cellular and developmental functions.

Materials and Methods

Ethics Statement

All zebrafish experiments in this research were carried out in accordance with the recommendations of, and were approved by, *hmx3a*^{SU3} single mutant either the UK Home Office or the Syracuse University IACUC committee.

Zebrafish Husbandry and Fish Lines

Zebrafish (*Danio rerio*) were maintained on a 14-h light/10-h dark cycle at 28.5°C. Embryos were obtained from natural paired and/or grouped spawnings of wild-type (WT; AB, TL or AB/TL hybrid) fish, heterozygous or homozygous *hmx2*, *hmx3a* or *hmx2/3a* mutants (reported here, see Fig. 4), *Tg*(*evx1:EGFP*)^{SU1} or *Tg*(*evx1:EGFP*)^{SU2} transgenic fish (Juárez-Morales et al., 2016), *Tg(UAS:mRFP*) transgenic fish (Balciuniene et al., 2013), heterozygous *mindbomb (mib*^{ta52}*)* mutants (Jiang et al., 1996) or heterozygous or homozygous *hmx3a*^{sa23045} mutants (Kettleborough et al., 2013).

CRISPR Mutagenesis and Screening

The generation of the *hmx3a*^{SU3} allele was previously described (Hartwell et al., 2019). With the exception of *hmx3a*^{sa23054} (which was generated as part of the Zebrafish Mutation Project and obtained from ZIRC), we generated all of the other *hmx2, hmx3a* and *hmx2/3a* mutants described in this paper using CRISPR mutagenesis. Single guide RNA (sgRNA) design and synthesis, plus *Cas9* mRNA synthesis was performed as described in (Hartwell et al., 2019). See Table 7 for sgRNA sequences used. *hmx2*^{SU35}*, hmx2*^{SU36}*, hmx2*^{SU37} and *hmx3a*^{SU42} alleles were all generated with a single sgRNA. *hmx2*^{SU38}*, hmx2*^{SU39}*, hmx2;hmx3a*^{SU44} and *hmx2;hmx3a*^{SU45} alleles are all deletions, generated by the combinatorial use of two sgRNA's. For *hmx2*^{SU39} we designed sgRNAs that flanked the homeodomain. For *hmx2*^{SU39} we used the same 3' sgRNA and a 5' sgRNA that was more 5' in the *hmx2* coding sequence. In the case of *hmx2;hmx3a,* which are adjacent on chromosome 17, we designed sgRNAs that flanked the two genes. To create these mutants, we injected 2-4 nl of a mixture of 200 ng/µl of each sgRNA + 600 ng/µl *nls-ZCas9-nls* mRNA into the single-cell of a one-cell stage AB WT embryo. *hmx3a*^{SU43} is a *hsp70:Gal4* knock-in allele. We co-injected a donor template containing *Gal4*, under the control of a minimal *hsp70* promoter, (Mbait-hsp70:Gal4, a kind gift of Dr Shin-ichi Higashijima, (Kimura et al., 2014)) with two sgRNA molecules: one specifically targeting *hmx3a* (see Table 7), and one, (*Mbait* sgRNA (GGCTGCTGCGGTTCCAGAGGTGG)), specifically linearizing the donor template *in vivo*, in to the single-cell of one-cell stage embryos derived from an incross of heterozygous *Tg(UAS:mRFP)* fish. For these experiments, the embryos were injected with 2-4 nl of a mixture of 130 ng/µl of each sgRNA + 180 ng/µl *nlz-ZCas9-nls* mRNA + 66 ng/µl *pMbait-hsp70:Gal4* donor DNA. The success of the knock-in was assessed by screening the injected embryos for RFP fluorescence in patterns consistent with *hmx3a* expression (i.e. in the ear, lateral line primordium and/or spinal cord) from 1 day post fertilization (dpf) onwards. We raised injected embryos displaying appropriate

expression patterns to adulthood and assessed for germline transmission of the knock-in allele by outcrossing to heterozygous or homozygous *Tg(UAS:mRFP)* fish. Note that Gal4 expression in *hmx3a*^{SU43} recapitulates *hmx3a* expression in the spinal cord, but not in the ear or lateral line primordium (data not shown).

We identified founder fish for *hmx2*^{SU35}, *hmx2*^{SU36}, *hmx2*^{SU37}, and *hmx3a*^{SU42} alleles using high resolution melt analysis (HRMA), and the supermix and amplification programs described in (Hartwell et al., 2019). See Table 7 for specific HRMA primer sequences. For the PCRs described below, we used Phusion High-Fidelity DNA Polymerase (M0530L, NEB) unless otherwise stated. All of the PCR primers used for each reaction are included in Table 1. We identified ***hmx2***^{SU38} founder fish by PCR, using the following conditions: 98.0°C for 30 seconds, 35 cycles of: 98.0°C for 10 seconds, 67.0°C for 30 seconds, 72.0°C for 40 seconds, followed by a final extension at 72.0°C for 5 minutes. The deletion in the mutant allele was distinguished by gel electrophoresis on a 1% TAE agarose gel (110V for 30 minutes). The WT allele generated a 1098 bp product, compared with a 671 bp mutant allele product. We identified ***hmx2***^{SU39} founder fish by nested PCR, using the following conditions: Nested PCR 1: 98.0°C for 30 seconds, 35 cycles of: 98.0°C for 10 seconds, 69.0°C for 20 seconds, 72.0°C for 75 seconds, followed by a final extension at 72.0°C for 5 minutes. The deletion in the mutant allele was distinguished by gel electrophoresis on a 1% TAE agarose gel (110V for 30 minutes). The WT allele generated a 2012 bp product (which may be detected on the gel), compared with a 576 bp mutant allele product. We then diluted the nested 1 PCR product 1:5 in sterile distilled water and performed the Nested PCR2 reaction using the following conditions: 98.0°C for 30 seconds, 35 cycles of: 98.0°C for 10 seconds, 66.0°C for 20 seconds, 72.0°C for 60 seconds, followed by a final extension at 72.0°C for 5 minutes. The deletion in the mutant allele was distinguished by gel electrophoresis on a 1% TAE agarose gel (110V for 30 minutes). The WT allele generated a 1758 bp product compared with a 322 bp mutant allele product. We identified ***hmx3a***^{SU43} founder fish either by screening for germline transmission (as described above) or using PCR with the following conditions: 98.0°C for 30 seconds, 35 cycles of: 98.0°C for 10 seconds, 69.0°C for 20 seconds, 72.0°C for 60 seconds, followed by a final extension at 72.0°C for 5 minutes. The deletion in the mutant allele was distinguished by gel electrophoresis on a 1% TAE agarose gel (110V for 30 minutes). A 1471 bp PCR product was only generated by fish heterozygous for the allele. It was not produced from WT animals since the reverse primer recognizes the inserted donor DNA sequence. We identified ***hmx2;hmx3a***^{SU44} and ***hmx2;hmx3a***^{SU45} founder fish by nested PCR, using the following conditions: Nested PCR 1: 98.0°C for 30 seconds, 35 cycles of: 98.0°C for 10 seconds, 67.0°C for 20 seconds, 72.0°C for 30 seconds, followed by a final extension at 72.0°C for 5 minutes. The deletion in the mutant allele was distinguished by gel electrophoresis on a 1% TAE agarose gel (110V for 30 minutes). The WT product was too large to be generated by these PCR conditions, so only heterozygous animals are detected by the presence of a 514 bp product on the gel. We then diluted the nested 1 PCR 1:5 in sterile distilled water and performed the Nested PCR2 reaction using the following conditions: 98.0°C for 30 seconds, 35 cycles of: 98.0°C for 10 seconds, 66.0°C for 20 seconds, 72.0°C for 30 seconds, followed by a final extension at 72.0°C for 5 minutes. The deletion in the mutant allele was distinguished by gel electrophoresis on a 1% TAE agarose gel (110V for 30 minutes). Again, the WT product

was too large to be generated by these PCR conditions, so only heterozygous animals were detected by the presence of a 445 bp product on the gel.

Once stable lines were established, we identified ***hmx2***^{SU35} fish by PCR, followed by sequencing (the mutation introduces a 1 bp insertion that cannot be resolved by restriction digestion, and we cannot distinguish heterozygotes from homozygotes using HRMA). We performed this PCR using Taq DNA Polymerase (M0320S, NEB) and the following conditions: 95.0ºC for 30 seconds, 35 cycles of: 95.0ºC for 20 seconds, 52.0ºC for 30 seconds, 68.0ºC for 45 seconds, followed by a final extension at 68.0ºC for 5 minutes. We identified ***hmx2***^{SU36} stable mutants by HRMA using the conditions described above. Homozygous mutants segregate from heterozygous animals by the scale of their deflection in the HRMA plot. ***hmx2***^{SU37} mutants were identified by performing the PCR used to sequence *hmx2*^{SU35} stable mutants (see above). When we analyzed the products on a 1% TAE gel (110V for 30 minutes), the WT allele generated a 580 bp product, compared with a 528 bp mutant allele product. We identified ***hmx2***^{SU38} stable mutants using the same PCR conditions initially used to identify founders (see above). We used the same nested PCR conditions to identify ***hmx2***^{SU39} mutants. However, the WT product was not always visible on the gel. Therefore, we also performed a WT amplicon PCR to detect a genomic region that only persists in WT and heterozygous animals. The WT amplicon PCR was identical to that described above for identifying stable *hmx2*^{SU35} fish. WT animals generated a WT amplicon PCR product, heterozygous animals generated both a WT amplicon PCR and Nested 2 PCR amplicon and homozygous animals generated the Nested 2 PCR amplicon but not the WT amplicon PCR product. We identified stable ***hmx3a***^{SU42} mutants by PCR, using Taq DNA Polymerase (M0320S, NEB) and the following conditions: 94.0ºC for 2 minutes, 35 cycles of: 94.0ºC for 30 seconds, 64.9ºC for 30 seconds, 72.0ºC for 30 seconds, followed by a final extension at 72.0ºC for 2 minutes. Whilst the mutant PCR product (321 bp) could sometimes be distinguished from the WT product (331 bp) by running on a 2% TBE gel (100V for 55 minutes), the mutation also deletes a BanI restriction site. Following digestion with BanI (R0118S, NEB), the products were run on a 2% TBE gel (100V for 40 minutes). The WT amplicon digested to completion, producing 120 bp + 211 bp bands, whereas the mutant product did not cut. We identified stable ***hmx3a***^{SU3} mutants by running the same PCR used to identify *hmx3a*^{SU42} mutants. The insertion in *hmx3a*^{SU3} was easily visualized on a 2% TBE gel. The WT product was 331 bp, compared to a mutant product of 400 bp. Since the PCR used to detect ***hmx3a***^{SU43} mutants was specific to the inserted donor DNA, and the WT amplicon in *hmx2;hmx3a*^{SU44} and *hmx2;hmx3a*^{SU45} mutants was too large to detect by standard PCR, we also performed a WT amplicon PCR to distinguish WTs from hets. For these alleles, the WT amplicon PCR was identical to that performed prior to BanI digestion on *hmx3a*^{SU42} mutants (see above). For *hmx3a*^{SU43}, the WT amplicon PCR results were compared to the PCR results (identical PCR to that first used to identify founders, see above), and for ***hmx2;hmx3a***^{SU44} and ***hmx2;hmx3a***^{SU45}, the WT amplicon PCR results were compared to the Nested 2 PCR results (identical Nested 2 PCR to that first used to identify founders – see above). In all cases, WT animals generated a WT amplicon PCR product, heterozygous animals generated both a WT amplicon and a

Nested PCR 2 amplicon product and homozygous animals generated the PCR / Nested 2 PCR amplicon but not the WT amplicon PCR product.

In all cases, stable F1 heterozygous fish were confirmed by sequencing. Where possible (see Fig. 4), to further confirm the mutant sequences, incrosses of homozygous viable adults were performed and the total RNA extracted using TRIzol Reagent (15596018, ThermoFisher Scientific) and the RNEasy Mini Kit (74104, Qiagen). Total RNA was converted to cDNA using the iScript cDNA synthesis kit (1708891, Bio-Rad). We performed Transcript-specific PCRs using the following primers and conditions: *hmx2*-FW: TGAACTGTTATGAGACGAGAATGAA and *hmx2*-RV: GTGTATTTTGTACGTCTTAGTGTGTGT (PCR: 98.0ºC for 30 seconds; 35 cycles of: 98.0ºC for 10 seconds, 64.2ºC for 20 seconds; 72.0ºC for 30 seconds, followed by final extension at 72.0ºC for 5 minutes) or *hmx3a*-FW: AACCGCGTTTAAGTTCCCATTG and *hmx3a*-RV: GTGCGAGTAGTAAACCGGATGAG (PCR: 98.0ºC for 30 seconds; 35 cycles of: 98.0ºC for 10 seconds, 71.0ºC for 20 seconds; 72.0ºC for 30 seconds, followed by final extension at 72.0ºC for 5 minutes). We then confirmed these homozygous mutant transcript sequences by sequencing. For those mutants which are not homozygous viable (*hmx3a*^{SU3}; *hmx3a*^{SU43}, *hmx2;hmx3a*^{SU44} and *hmx2;hmx3a*^{SU45}), progeny from incrosses of heterozygous animals were examined for otolith fusion phenotypes (see below). homozygous mutant embryos with fused otoliths were pooled and their total RNA extracted and converted to cDNA, prior to PCR as described above. See Fig. 4 for details of how individual mutant alleles differ from one another.

Morpholino injections

For single knockdown (SKD) experiments, 3.5 nl of a mixture containing either 2 ng/nl of a translation-blocking *hmx2* morpholino (5' TTCCGCTGTCCTCCGAATTATTCAT) or 2 ng/nl of a translation-blocking *hmx3a* morpholino (5' ACGTATCCTGTGTTGTTTCGGGCAT) plus 5 ng/nl of a control zebrafish p53 morpholino (5' GCGCCATTGCTTTGCAAGAATTG) was injected in to the single-cell of a one-cell stage WT embryo (all morpholinos were purchased from Gene Tools). For double knockdown (DKD) experiments, 3.5 nl of a mixture containing 2 ng/nl of both *hmx* morpholinos plus 5 ng/nl of the control zebrafish p53 morpholino was injected. DKD but not SKD embryos exhibit delayed development from somitogenesis stages onwards when compared to uninjected controls. To circumvent this, DKD embryos were incubated at 32ºC from 9 hours post fertilization (h) onwards. This ensured that control and injected embryos reached the desired developmental stage of 27 h at approximately the same time. The lateral line primordium does not migrate in DKD animals, so this cannot be used to stage the injected embryos. Instead, these embryos were visually inspected and fixed when they displayed the same head-trunk angle, head size and eye size as prim-staged uninjected control embryos (Kimmel, 1995). Migration of the lateral line primordium is unaffected in SKD embryos and so these were prim-staged prior to fixing for experiments (Kimmel, 1995). Morpholino injections always produce a spectrum of phenotypes, since it is hard to ensure that every cell receives the same dose. Therefore, prior to fixing at 27 h, we removed any embryos with severely abnormal morphology (stunted length and/or severely developmentally delayed - likely caused by

receiving too much morpholino). Embryos injected with *hmx2/3* morpholinos (SKD and DKD) display a slight curled-tail-down morphology. Embryos that lacked this morphology (and may therefore not have received any or sufficient morpholino) were also removed before fixing.

For the mRNA rescue experiments, we co-injected both morpholinos (at the same volume and dose described above), together with a total dose of up to 500 pg of morpholino resistant *hmx3a* mRNA. This mRNA had 7 nucleotides altered in the *hmx3* morpholino recognition sequence. Each change was in the third nucleotide of a codon. This codon wobble was used so that the same amino acid was encoded in each case, but the mRNA would not be recognized by the morpholino. The protein encoded by the injected RNA is therefore the same as endogenous Hmx3a.

To assess whether genetic compensation might be occurring in either *hmx3a*^{SU42} mutants, which lack obvious phenotypes (see Fig. 4), or *hmx3a*^{SU3} mutants, which have milder spinal cord phenotypes than *hmx2/3a* DKD embryos (compare Figs 3 and 5), we injected the same dose of *hmx3a* + *p53* MOs as described above in to the single-cell of one-cell stage embryos generated from incrosses of either heterozygous *hmx3a*^{SU42} or *hmx3a*^{SU3} parents. If genetic compensation is occurring, the upregulated compensating gene(s) will not be knocked-down by the *hmx3a* morpholino and the phenotype of homozygous mutants should be unchanged. In contrast, WT and heterozygous animals, which contain at least one WT copy of *hmx3a*, will be susceptible to the *hmx3a* morpholino and should exhibit stronger, morphant-like phenotypes. For these experiments, while we removed any embryos with severely abnormal morphology, we did not remove embryos that lacked the curled-tail-down morphology, incase these were morpholino-resistant mutant embryos. After fixing, we performed an *in situ* hybridization for the glutamatergic marker, *slc17a6a/b*. We visually inspected the embryos on a dissecting microscope and categorized as to whether they displayed the stronger, morphant-like phenotype (large reduction in the number of *slc17a6a/b*-expressing cells) or mutant-like phenotype (WT-like in the case of *hmx3a*^{SU42} or more subtle reduction in the number of *slc17a6a/b*-expressing cells in the case of *hmx3a*^{SU3} embryos). Embryos within each class were then genotyped as described in the CRISPR mutagenesis section above.

Genotyping

We isolated DNA for genotyping from both anesthetized adult fish and fixed embryos via fin biopsy or head dissections, respectively. We genotyped the *hmx* CRISPR mutants as described in the CRISPR mutagenesis section above. For *mib*^{ta52b} and *hmx3a*^{sa23054} mutants, we used KASP assays designed by LGC Genomics LLC. KASP assays use allele-specific PCR primers, which differentially bind fluorescent dyes that we quantified with a BioRad CFX96 real-time PCR machine to distinguish genotypes. The proprietary primers used were: *mib_ta52b* and *hmx3a_sa23054*. Heads of fixed embryos were dissected in 70% glycerol/30% phosphate-buffered saline (PBS) with insect pins. Embryo trunks were stored in 70% glycerol/30% PBS at 4°C for later analysis. DNA was

extracted via the HotSHOT method (Truett et al., 2000) using 10 µl of 50 mM NaOH and 1 µl of 1M Tris-HCl (pH-7.4).

in situ hybridization and immunohistochemistry

We fixed embryos in 4% paraformaldehyde and performed single and double *in situ* hybridizations and immunohistochemistry plus *in situ* hybridization double labeling experiments as previously described (Batista et al., 2008; Concordet et al., 1996). Sources of *in situ* hybridization probes are provided in Table 1. To amplify *in situ* hybridization probe templates for *hmx1* and *hmx3b*, we created zebrafish cDNA from 27 h WT zebrafish embryos. We extracted total RNA by homogenizing 50–100 mg of embryos in 1 mL of TRIzol reagent (Ambion, 15596-026). We confirmed RNA integrity (2:1 ratio of 28S:18S rRNA bands) and quality (A260/A280 ratio of ~2.0) using agarose gel electrophoresis and spectrophotometry respectively. We synthesized cDNA using Bio-Rad iScript Reverse Transcription Supermix kit (Bio-Rad, 170-8891). We amplified *hmx1* sequence from the cDNA using Phusion High-Fidelity DNA Polymerase (M0530L, NEB), primers *hmx1*-FW: CTGGTATATTTGCTCAAGACATGC and *hmx1*-RV: GCTTCTGCTGAACACAGTTCG and PCR conditions: 98.0ºC for 10 seconds, 30 cycles of: 98.0ºC for 6 seconds; 57.0ºC for 30 seconds and 72.0ºC for 30 seconds, followed by a final extension for 45 seconds at 72.0ºC. The PCR product was assessed on a 1% TAE gel, before purifying with QIAquick PCR Purification Kit (28104, Qiagen). We used Taq DNA Polymerase (M0320S, NEB) to add 3'A overhangs prior to TOPO TA-cloning (K4600-01, Invitrogen). We then performed colony PCR using the same PCR primers and conditions used to amplify the *hmx1* sequence from cDNA. We extracted Plasmid DNA from positive colonies using QIAprep Spin Miniprep Kit (27104, Qiagen) and then verified the sequence using standard SP6 and T7 primer sequences. To make the anti-sense RNA riboprobe, we linearized DNA with HindIII-HF (R3104S, NEB) and transcribed with T7 RNA Polymerase (10881767001, Roche). We used a PCR-based DNA template to make the *hmx3b* ISH probe. The reverse primer contains the T3 RNA Polymerase minimal promoter sequence (underlined). We used primers *hmx3b*-FW: GTGTGCCCGTCATCTACCAC and *hmx3b*-RV: AATTAACCCTCACTAAAGGGATGAAGATGATGAAGATGCGCAAC, 27 h cDNA, Phusion High-Fidelity DNA Polymerase (M0530L, NEB) and PCR conditions: 94.0ºC for 3 minutes, 35 cycles of: 94.0ºC for 30 seconds, 56.5ºC for 30 seconds and 72.0ºC for 1.5 minutes, followed by a final extension step of 72.0ºC for 10 minutes. We purified the template through phenol:chloroform extraction prior to *in situ* probe synthesis using 1 µg purified PCR product, T3 RNA Polymerase (11031171001, Roche) and DIG RNA Labeling Mix (11277073910, Roche).

Embryos older than 24 h were usually incubated in 0.003% 1- phenyl-2-thiourea (PTU) to prevent pigment formation. For some experiments we added 5% of dextran sulphate to the hybridization buffer (Table 2). Dextran sulphate can increase specific staining in *in situ* hybridization experiments as it facilitates molecular crowding (Ku et al., 2004; Lauter et al., 2011).

In cases where we did not detect expression of a particular gene in the spinal cord, we checked for low levels of expression by exposing embryos to prolonged staining. In some cases, this produced higher background (diffuse, non-specific staining), especially in the hindbrain, where ventricles can sometimes trap anti-sense riboprobes.

To determine neurotransmitter phenotypes we used probes for genes that encode proteins that transport or synthesize specific neurotransmitters as these are some of the most specific molecular markers of these cell fates (Higashijima et al., 2004b; Higashijima et al., 2004c and references therein). A mixture of probes to *slc17a6a* and *slc17a6b* (previously called *vglut*), which encode glutamate transporters, was used to label glutamatergic neurons (Higashijima et al., 2004b; Higashijima et al., 2004c). GABAergic neurons were labeled using probes to *gad1b* (probes previously called *gad67a* and *gad67b*) (Higashijima et al., 2004b; Higashijima et al., 2004c). The *gad1b* gene encodes for a glutamic acid decarboxylase, which is necessary for the synthesis of GABA from glutamate. A mixture of probes (*glyt2a* and *glyt2b*) for *slc6a5* (previously called *glyt2*) was used to label glycinergic cells (Higashijima et al., 2004b; Higashijima et al., 2004c). *slc6a5* encodes for a glycine transporter necessary for glycine reuptake and transport across the plasma membrane.

The antibodies that we used for fluorescent *in situ* hybridization were mouse anti-Dig (200-002-156, Jackson ImmunoResearch, 1:5000) and rabbit anti-Flu (A889, Invitrogen, 1:2500). These were detected using secondary antibodies goat anti-rabbit-HRP (G-21234, ThermoFisher Scientific, 1:750) and goat anti-mouse-HRP (G-21040, ThermoFisher Scientific, 1:750) and Tyramide SuperBoost Kits B40922 and B40915 (ThermoFisher Scientific).

For fluorescent *in situ* hybridization + immunohistochemistry, after detection of the *in situ* hybridization reaction using Tyramide SuperBoost Kit B40915, with HRP, Goat anti-mouse IgG and Alexa Fluor 594 Tyramide), embryos were washed 8 × 15min in PBST (PBS with 0.1% Tween-20) and incubated in Image-iT FX Signal Enhancer (ThermoFisher Scientific, I36933) for 30min at room temperature. Immunohistochemistry was performed using chicken polyclonal anti-GFP primary antibody (Ab13970, Abcam, 1:500) and a Goat anti-chicken IgY (H+L), Alexa Fluor 488 secondary antibody (A-11039, ThermoFisher Scientific, 1:1000).

<u>Screening lateral line and otolith phenotypes</u>

We examined whether any of the *hmx* mutants generated in this study had lateral line and/or fused otolith phenotypes, as reported for *hmx2;hmx3a* double-knockdown embryos (Feng and Xu, 2010). To assay live lateral line phenotypes, we anaesthetized embryos from incrosses of heterozygous mutant fish in 0.016% tricaine (A5040, Sigma Aldrich) in embryo medium and mounted them on coverslip bridges (2 x 22 mm square glass coverslips (16004-094, VWR) glued together on either side of a 24 x 60 mm glass cover slip (12460S, ThermoFisher Scientific), overlaid with a third 22 mm square glass coverslip). Using a Zeiss Axio Imager M1 compound microscope, we located the tip of the lateral line primordium and counted the somite number adjacent to this

position. We also used this method routinely to determine the developmental stage of embryos prior to fixing for *in situ* hybridization. To assay lateral line phenotypes in fixed embryos, we performed *in situ* hybridizations using anti-sense riboprobes for *hmx3a* or *krt15* (both of which label the migrating primordium and neuromasts) and then determined the lateral line position as in live embryos. To examine live otolith phenotypes, embryos were raised until 3 dpf, before anaesthetizing (as for assessing live lateral line phenotypes) and examining the spatial location of otoliths in both ears. WT embryos have two otoliths in each ear: one smaller, anterior otolith, and one larger, posterior otolith. These are separate from each other and spatially distinct. We classified otoliths as fused if only one large, amalgamated otolith was visible in a mid-ventral position within the otic vesicle (see Fig. 5E).

Imaging

Embryos were mounted in 70% glycerol, 30% PBS and DIC pictures were taken using an AxioCam MRc5 camera mounted on a Zeiss Axio Imager M1 compound microscope. Fluorescent images were taken on a Zeiss LSM 710 confocal microscope. Images were processed using Adobe Photoshop software (Adobe, Inc) and Image J software (Abramoff et al., 2004). In some cases, different focal planes were merged to show labeled cells at different medial lateral positions in the spinal cord. All images were processed for brightness-contrast and color balance using Adobe Photoshop software (Adobe, Inc.). Images of control and mutant embryos from the same experiment were processed identically. Figures were assembled using Adobe Photoshop and Adobe Illustrator (Adobe, Inc.).

Cell counts and statistics

In all cases, except where noted to the contrary, cell counts are for both sides of a five-somite length of spinal cord adjacent to somites 6-10. Embryos were mounted laterally with the somite boundaries on each side of the embryo exactly aligned and the apex of the somite over the middle of the notochord. This ensures that the spinal cord is straight along its dorsal-ventral axis and that cells in the same dorsal/ventral position on opposite sides of the spinal cord will be directly above and below each other. Embryos from single and double mutant crosses were counted blind to genotype. Labeled cells in embryos analyzed by DIC were counted while examining embryos on a Zeiss Axio Imager M1 compound microscope. We identified somites 6–10 in each embryo and counted the number of labeled cells in that stretch of the spinal cord. We adjusted the focal plane as we examined the embryo to count cells at all medial/lateral positions (both sides of the spinal cord; also see Batista et al., 2008; Batista and Lewis, 2008; England et al., 2011; Hilinski et al., 2016; Juárez-Morales et al., 2016).

In some cases, cell count data were pooled from different experiments. Prior to pooling, all pairwise combinations of data sets were tested to determine if there were any statistically significant differences between them as described below. Data were only pooled if none of the pairwise comparisons were statistically significantly different from each other. In addition, as *in situ* hybridization staining can vary slightly between experiments we only compared different mutant results when the counts from their corresponding WT sibling embryos were not statistically significantly different from each other.

To determine whether differences in values are statistically significant, data were first analyzed for normality using the Shapiro–Wilk test. Data sets with non-normal distributions were subsequently analyzed using the Wilcoxon (Mann–Whitney) test. For data sets with normal distributions, the F-test for equal variances was performed, prior to conducting either a type 2 (for equal variances) or type 3 (for non-equal variances) student's *t*-test. P values generated by Wilcoxon, type 2 student's *t*-test and type 3 student's *t*-test are indicated by $^{\wedge}$, $^{+}$ and § respectively. *n*-values for each experiment are provided in the figure legends. To assess whether mutant phenotypes occurred at Mendelian frequencies, we perfomed Chi-squared tests.

Microarray expression profiling experiments

These experiments are described in detail in (Cerda et al., 2009). P values were corrected for multiple testing (Benjamini and Hochberg, 1995; Gentleman et al., 2004; Tarraga et al., 2008)

Acknowledgments

We thank ZFIN for providing information on nomenclature and other essential zebrafish resources and Henry Putz, Jessica Bouchard, Paul Campbell, Annika Swanson and several SU undergraduate fish husbandry workers for help with maintaining zebrafish lines. This research was funded by NINDS R01:NS077947.

Author Contributions

SJE created all the *hmx* mutants described in this study except *hmx3a*^{sa23054}, performed most of the morpholino and mutant experiments, all of the statistical analyses and prepared the figures and some of the tables; GAC performed most of the double-labelling experiments and some of the morpholino analyses; AK, TS and GG performed some of the genotyping and *in situ* hybridization experiments and AK also performed some of the double-labelling experiments; KEL conceptualized and directed the study, acquired the financial support for the project, contributed to data analysis, made some of the tables and wrote the paper. All authors read and commented on drafts of the paper and approved the final version.

References

Adamska, M., Leger, S., Brand, M., Hadrys, T., Braun, T. and Bober, E. (2000). Inner ear and lateral line expression of a zebrafish Nkx5-1 gene and its downregulation in the ears of FGF8 mutant, ace. *Mechanisms of development* **97**, 161-165.

Alaynick, W. A., Jessell, T. M. and Pfaff, S. L. (2011). SnapShot: spinal cord development. *Cell* **146**, 178-178 e171.

Balciuniene, J., Nagelberg, D., Walsh, K. T., Camerota, D., Georlette, D., Biemar, F., Bellipanni, G. and Balciunas, D. (2013). Efficient disruption of Zebrafish genes using a Gal4-containing gene trap. *Bmc Genomics* **14**, 619.

Batista, M. F., Jacobstein, J. and Lewis, K. E. (2008). Zebrafish V2 cells develop into excitatory CiD and Notch signalling dependent inhibitory VeLD interneurons. *Dev Biol* **322**, 263-275.

Batista, M. F. and Lewis, K. E. (2008). Pax2/8 act redundantly to specify glycinergic and GABAergic fates of multiple spinal interneurons. *Dev Biol* **323**, 88-97.

Benjamini, Y. and Hochberg, Y. (1995). Controlling the false discovery rate: a practical and powerful approach to multiple testing. *Journal of the Royal Statistical Society Series B* **57**, 289–300.

Bober, E., Baum, C., Braun, T. and Arnold, H. H. (1994). A novel NK-related mouse homeobox gene: expression in central and peripheral nervous structures during embryonic development. *Dev Biol* **162**, 288-303.

Boisset, G. and Schorderet, D. F. (2012). Zebrafish hmx1 promotes retinogenesis. *Exp Eye Res* **105**, 34-42.

Burglin, T. R. and Affolter, M. (2016). Homeodomain proteins: an update. *Chromosoma* **125**, 497-521.

Carrasco, A. E., McGinnis, W., Gehring, W. J. and De Robertis, E. M. (1984). Cloning of an X. laevis gene expressed during early embryogenesis coding for a peptide region homologous to Drosophila homeotic genes. *Cell* **37**, 409-414.

Cerda, G. A., Hargrave, M. and Lewis, K. E. (2009). RNA profiling of FAC-sorted neurons from the developing zebrafish spinal cord. *Developmental dynamics : an official publication of the American Association of Anatomists* **238**, 150-161.

Cheng, L., Arata, A., Mizuguchi, R., Qian, Y., Karunaratne, A., Gray, P. A., Arata, S., Shirasawa, S., Bouchard, M., Luo, P., et al. (2004). Tlx3 and Tlx1 are post-mitotic selector genes determining glutamatergic over GABAergic cell fates. *Nature neuroscience* **7**, 510-517.

Cheng, L., Samad, O. A., Xu, Y., Mizuguchi, R., Luo, P., Shirasawa, S., Goulding, M. and Ma, Q. (2005). Lbx1 and Tlx3 are opposing switches in determining GABAergic versus glutamatergic transmitter phenotypes. *Nature neuroscience* **8**, 1510-1515.

Concordet, J. P., Lewis, K. E., Moore, J. W., Goodrich, L. V., Johnson, R. L., Scott, M. P. and Ingham, P. W. (1996). Spatial regulation of a zebrafish patched homologue reflects the roles of sonic hedgehog and protein kinase A in neural tube and somite patterning. *Development* **122**, 2835-2846.

Delile, J., Rayon, T., Melchionda, M., Edwards, A., Briscoe, J. and Sagner, A. (2019). Single cell transcriptomics reveals spatial and temporal dynamics of gene expression in the developing mouse spinal cord. *Development* **146**.

El-Brolosy, M. A., Kontarakis, Z., Rossi, A., Kuenne, C., Gunther, S., Fukuda, N., Kikhi, K., Boezio, G. L. M., Takacs, C. M., Lai, S. L., et al. (2019). Genetic compensation triggered by mutant mRNA degradation. *Nature* **568**, 193-197.

El-Brolosy, M. A. and Stainier, D. Y. R. (2017). Genetic compensation: A phenomenon in search of mechanisms. *PLoS genetics* **13**, e1006780.

England, S., Batista, M. F., Mich, J. K., Chen, J. K. and Lewis, K. E. (2011). Roles of Hedgehog pathway components and retinoic acid signalling in specifying zebrafish ventral spinal cord neurons. *Development* **138**, 5121-5134.

England, S. J., Campbell, P. C., Banerjee, S., Swanson, A. J. and Lewis, K. E. (2017). Identification and Expression Analysis of the Complete Family of Zebrafish pkd Genes. *Front Cell Dev Biol* **5**, 5.

Feng, Y. and Xu, Q. (2010). Pivotal role of hmx2 and hmx3 in zebrafish inner ear and lateral line development. *Dev Biol* **339**, 507-518.

Fortunato, S. A., Adamski, M., Ramos, O. M., Leininger, S., Liu, J., Ferrier, D. E. and Adamska, M. (2014). Calcisponges have a ParaHox gene and dynamic expression of dispersed NK homeobox genes. *Nature* **514**, 620-623.

French, C. R., Erickson, T., Callander, D., Berry, K. M., Koss, R., Hagey, D. W., Stout, J., Wuennenberg-Stapleton, K., Ngai, J., Moens, C. B., et al. (2007). Pbx homeodomain proteins pattern both the zebrafish retina and tectum. *BMC developmental biology* **7**, 85.

Gehring, W. J. (1985). The homeo box: a key to the understanding of development? *Cell* **40**, 3-5.

Gentleman, R. C., Carey, V. J., Bates, D. M., Bolstad, B., Dettling, M., Dudoit, S., Ellis, B., Gautier, L., Ge, Y., Gentry, J., et al. (2004). Bioconductor: open software development for computational biology and bioinformatics. *Genome biology* **5**, R80.

Gongal, P. A., March, L. D., Holly, V. L., Pillay, L. M., Berry-Wynne, K. M., Kagechika, H. and Waskiewicz, A. J. (2011). Hmx4 regulates Sonic hedgehog signaling through control of retinoic acid synthesis during forebrain patterning. *Dev Biol* **355**, 55-64.

Gowan, K., Helms, A. W., Hunsaker, T. L., Collisson, T., Ebert, P. J., Odom, R. and Johnson, J. E. (2001). Crossinhibitory activities of Ngn1 and Math1 allow specification of distinct dorsal interneurons. *Neuron* **31**, 219-232.

Gross, M. K., Dottori, M. and Goulding, M. (2002). Lbx1 specifies somatosensory association interneurons in the dorsal spinal cord. *Neuron* **34**, 535-549.

Grossmann, K. S., Giraudin, A., Britz, O., Zhang, J. and Goulding, M. (2010). Genetic Dissection of Rhythmic Motor Networks in Mice. *Progress in Brain Research* **187**, 19-37.

Hartwell, R. D., England, S. J., Monk, N. A. M., van Hateren, N. J., Baxendale, S., Marzo, M., Lewis, K. E. and Whitfield, T. T. (2019). Anteroposterior patterning of the zebrafish ear through Fgf- and Hh-dependent regulation of hmx3a expression. *PLoS genetics* **15**, e1008051.

Higashijima, S., Masino, M. A., Mandel, G. and Fetcho, J. R. (2004a). Engrailed-1 expression marks a primitive class of inhibitory spinal interneuron. *J Neurosci* **24**, 5827-5839.

Higashijima, S., Schaefer, M. and Fetcho, J. R. (2004b). Neurotransmitter properties of spinal interneurons in embryonic and larval zebrafish. *J Comp Neurol* **480**, 19-37.

Higashijima, S. I., Mandel, G. and Fetcho, J. R. (2004c). Distribution of prospective glutamatergic, glycinergic, and gabaergic neurons in embryonic and larval zebrafish. *Journal of Comparative Neurology* **480**, 1-8.

Higashijima, S. I., Schaefer, M. and Fetcho, J. R. (2004d). Neurotransmitter properties of spinal interneurons in embryonic and larval zebrafish. *Journal of Comparative Neurology* **480**, 19-37.

Hilinski, W. C., Bostrom, J. R., England, S. J., Juárez-Morales, J. L., de Jager, S., Armant, O., Legradi, J., Strähle, U., Link, B. A. and Lewis, K. E. (2016). Lmx1b is required for the glutamatergic fates of a subset of spinal cord neurons. *Neural development* **11**, 16.

Holland, P. W. (2013). Evolution of homeobox genes. *Wiley Interdiscip Rev Dev Biol* **2**, 31-45.

Itoh, M., Kim, C., Palardy, G., Oda, T., Jiang, Y., Maust, D., Yeo, S., Lorick, K., Wright, G., Ariza-McNaughton, L., et al. (2003). Mind bomb is a ubiquitin ligase that is essential for efficient activation of Notch signaling by Delta. *Dev Cell.* **4**, 67-82.

Jiang, Y. J., Brand, M., Heisenberg, C. P., Beuchle, D., Furutani-Seiki, M., Kelsh, R. N., Warga, R. M., Granato, M., Haffter, P., Hammerschmidt, M., et al. (1996). Mutations affecting neurogenesis and brain morphology in the zebrafish, *Danio rerio*. *Development* **123**, 205-216.

Juárez-Morales, J. L., Schulte, C. J., Pezoa, S. A., Vallejo, G. K., Hilinski, W. C., England, S. J., de Jager, S. and Lewis, K. E. (2016). Evx1 and Evx2 specify excitatory neurotransmitter fates and suppress inhibitory fates through a Pax2-independent mechanism. *Neural development* **11**, 5.

Kettleborough, R. N. W., Busch-nentwich, E. M., Harvey, S. A., Dooley, C. M., Bruijn, E. D., Eeden, F. V., Sealy, I., White, R. J., Herd, C., Nijman, I. J., et al. (2013). A systematic genome-wide analysis of zebrafish protein-coding gene function. **496**, 494-497.

Kimmel, C. B. (1995). Stages of Embryonic Development of the Zebrafish

Kimura, Y., Hisano, Y., Kawahara, A. and Higashijima, S. (2014). Efficient generation of knock-in transgenic zebrafish carrying reporter/driver genes by CRISPR/Cas9-mediated genome engineering. *Scientific reports* **4**, 6545.

Kimura, Y., Okamura, Y. and Higashijima, S. (2006). alx, a zebrafish homolog of Chx10, marks ipsilateral descending excitatory interneurons that participate in the regulation of spinal locomotor circuits. *J Neurosci* **26**, 5684-5697.

Ku, W. C., Lau, W. K., Tseng, Y. T., Tzeng, C. M. and Chiu, S. K. (2004). Dextran sulfate provides a quantitative and quick microarray hybridization reaction. *Biochemical and biophysical research communications* **315**, 30-37.

Larroux, C., Fahey, B., Degnan, S. M., Adamski, M., Rokhsar, D. S. and Degnan, B. M. (2007). The NK homeobox gene cluster predates the origin of Hox genes. *Current biology : CB* **17**, 706-710.

Lauter, G., Soll, I. and Hauptmann, G. (2011). Two-color fluorescent in situ hybridization in the embryonic zebrafish brain using differential detection systems. *BMC developmental biology* **11**, 43.

Marcelli, F., Boisset, G. and Schorderet, D. F. (2014). A dimerized HMX1 inhibits EPHA6/epha4b in mouse and zebrafish retinas. *PloS one* **9**, e100096.

Moran-Rivard, L., Kagawa, T., Saueressig, H., Gross, M. K., Burrill, J. and Goulding, M. (2001). Evx1 is a postmitotic determinant of V0 interneuron identity in the spinal cord. *Neuron* **29**, 385-399.

Muller, T., Anlag, K., Wildner, H., Britsch, S., Treier, M. and Birchmeier, C. (2005). The bHLH factor Olig3 coordinates the specification of dorsal neurons in the spinal cord. *Genes & development* **19**, 733-743.

Muller, T., Brohmann, H., Pierani, A., Heppenstall, P. A., Lewin, G. R., Jessell, T. M. and Birchmeier, C. (2002). The homeodomain factor lbx1 distinguishes two major programs of neuronal differentiation in the dorsal spinal cord. *Neuron* **34**, 551-562.

Park, H. C. and Appel, B. (2003). Delta-Notch signaling regulates oligodendrocyte specification. *Development* **130**, 3747-3755.

Peng, J. (2019). Gene redundancy and gene compensation: An updated view. *Journal of genetics and genomics* **46**, 329-333.

Pisani, D., Pett, W., Dohrmann, M., Feuda, R., Rota-Stabelli, O., Philippe, H., Lartillot, N. and Worheide, G. (2015). Genomic data do not support comb jellies as the sister group to all other animals. *Proc Natl Acad Sci U S A* **112**, 15402-15407.

Rossi, A., Kontarakis, Z., Gerri, C., Nolte, H., Holper, S., Kruger, M. and Stainier, D. Y. (2015). Genetic compensation induced by deleterious mutations but not gene knockdowns. *Nature* **524**, 230-233.

Satou, C., Kimura, Y. and Higashijima, S. (2012). Generation of multiple classes of V0 neurons in zebrafish spinal cord: progenitor heterogeneity and temporal control of neuronal diversity. *J Neurosci* **32**, 1771-1783.

Schier, A. F., Neuhauss, S. C. F., Harvey, M., Malicki, J., Solnica-Krezel, L., Stainier, D. Y. R., Zwartkruis, F., Abdelilah, S., Stemple, D. L., Rangini, Z., et al. (1996). Mutations affecting the development of the embryonic zebrafish brain. *Development* **123**, 165-178.

Simion, P., Philippe, H., Baurain, D., Jager, M., Richter, D. J., Di Franco, A., Roure, B., Satoh, N., Queinnec, E., Ereskovsky, A., et al. (2017). A Large and Consistent Phylogenomic Dataset Supports Sponges as the Sister Group to All Other Animals. *Current biology : CB* **27**, 958-967.

Sordino, P., Duboule, D. and Kondo, T. (1996). Zebrafish *Hoxa* and *Evx-2* genes: cloning, developmental expression and implications for the functional evolution of posterior *Hox* genes. *Mech. Dev.* **59**, 165 - 175.

Sztal, T. E., McKaige, E. A., Williams, C., Ruparelia, A. A. and Bryson-Richardson, R. J. (2018). Genetic compensation triggered by actin mutation prevents the muscle damage caused by loss of actin protein. *PLoS genetics* **14**, e1007212.

Talpalar, A. E., Bouvier, J., Borgius, L., Fortin, G., Pierani, A. and Kiehn, O. (2013). Dual-mode operation of neuronal networks involved in left-right alternation. *Nature* **500**, 85-88.

Tarraga, J., Medina, I., Carbonell, J., Huerta-Cepas, J., Minguez, P., Alloza, E., Al-Shahrour, F., Vegas-Azcarate, S., Goetz, S., Escobar, P., et al. (2008). GEPAS, a web-based tool for microarray data analysis and interpretation. *Nucleic acids research* **36**, W308-314.

Thaeron, C., Avaron, F., Casane, D., Borday, V., Thisse, B., Thisse, C., Boulekbache, H. and Laurenti, P. (2000). Zebrafish *evx1* is dynamically expressed during embryogenesis in subsets of interneurones, posterior gut and urogenital system. *Mechanisms of development* **99**, 167-172.

Topalidou, I., van Oudenaarden, A. and Chalfie, M. (2011). Caenorhabditis elegans aristaless/Arx gene alr-1 restricts variable gene expression. *Proc Natl Acad Sci U S A* **108**, 4063-4068.

Toyama, R. and Dawid, I. (1997). *lim6*, a novel LIM homeobox gene in the zebrafish: comparison of its expression pattern with *lim1*. *Dev. Dyn.* **209**, 406-417.

Treffkorn, S., Kahnke, L., Hering, L. and Mayer, G. (2018). Expression of NK cluster genes in the onychophoran Euperipatoides rowelli: implications for the evolution of NK family genes in nephrozoans. *Evodevo* **9**, 17.

Truett, G. E., Heeger, P., Mynatt, R. L., Truett, A. A., Walker, J. A. and Warman, M. L. (2000). Preparation of PCR-quality mouse genomic DNA with hot sodium hydroxide and tris (HotSHOT). *BioTechniques* **29**, 52, 54.

Valentin, G., Haas, P. and Gilmour, D. (2007). The chemokine SDF1a coordinates tissue migration through the spatially restricted activation of Cxcr7 and Cxcr4b. *Current biology : CB* **17**, 1026-1031.

Wang, W., Chan, E. K., Baron, S., Van de Water, T. and Lufkin, T. (2001). Hmx2 homeobox gene control of murine vestibular morphogenesis. *Development* **128**, 5017-5029.

Wang, W., Grimmer, J. F., Van De Water, T. R. and Lufkin, T. (2004). Hmx2 and Hmx3 homeobox genes direct development of the murine inner ear and hypothalamus and can be functionally replaced by Drosophila Hmx. *Developmental cell* **7**, 439-453.

Wang, W., Lo, P., Frasch, M. and Lufkin, T. (2000). Hmx: an evolutionary conserved homeobox gene family expressed in the developing nervous system in mice and Drosophila. *Mechanisms of development* **99**, 123-137.

Wang, W. and Lufkin, T. (2005). Hmx homeobox gene function in inner ear and nervous system cell-type specification and development. *Exp Cell Res* **306**, 373-379.

Wang, W., Van De Water, T. and Lufkin, T. (1998). Inner ear and maternal reproductive defects in mice lacking the Hmx3 homeobox gene. *Development* **125**, 621-634.

Wine-Lee, L., Ahn, K. J., Richardson, R. D., Mishina, Y., Lyons, K. M. and Crenshaw, E. B., 3rd (2004). Signaling through BMP type 1 receptors is required for development of interneuron cell types in the dorsal spinal cord. *Development* **131**, 5393-5403.

Wotton, K. R., Weierud, F. K., Juarez-Morales, J. L., Alvares, L. E., Dietrich, S. and Lewis, K. E. (2010). Conservation of gene linkage in dispersed vertebrate NK homeobox clusters. *Development genes and evolution* **219**, 481-496.

Zheng, C. and Chalfie, M. (2016). Securing Neuronal Cell Fate in C. elegans. *Curr Top Dev Biol* **116**, 167-180.

Zheng, C., Jin, F. Q. and Chalfie, M. (2015). Hox Proteins Act as Transcriptional Guarantors to Ensure Terminal Differentiation. *Cell Rep* **13**, 1343-1352.

Zhu, P., Ma, Z., Guo, L., Zhang, W., Zhang, Q., Zhao, T., Jiang, K., Peng, J. and Chen, J. (2017). Short body length phenotype is compensated by the upregulation of nidogen family members in a deleterious nid1a mutation of zebrafish. *Journal of genetics and genomics* **44**, 553-556.

Tables and Table Legends

Table 1.

Gene name	Previous names	ZFIN ID	Reference For Probe
hmx1	*nkx5.3,nkx5-3, im:7155045, zgc:172164*	ZDB-GENE-080204-54	This publication – see materials and methods.
hmx2	*nkx5.2*	ZDB-GENE-080506-2	Feng & Xu (2010)
hmx3a	*hmx3, Nkx5-1, nkx5.1, zgc:109845*	ZDB-GENE-001020-1	Feng & Xu (2010)
hmx3b	*si:zfos-911d5.2*	ZDB-GENE-130603-102	This publication – see materials and methods.
hmx4	*hmx3b, zfSOHo, wu:fc21b03, zgc:154104*	ZDB-GENE-060825-142	Feng & Xu (2010)
slc32a1	*viaat, zgc:158324*	ZDB-GENE-061201-1	Kimura *et al*., (2006)
en1b	*eng1b,eng4, engrailed 4, wu:fc84e11, zgc:113499*	ZDB-GENE-980526-6	Gift of Drs. Kikuci & Westerfield at the University of Oregon.
slc17a6a	*slc17a6l, VGLUT2.2, vglut2b, wu:fj12c01*	ZDB-GENE-050105-4	Higashijima *et al*., (2004b) Higashijima *et al*., (2004c)
slc17a6b	*slc17a6, blu, blumenkohl, si:packt73.2; si:packt90.2, si:xx-packt73.2, VGLUT2.1, vglut2a*	ZDB-GENE-030616-554	Higashijima *et al*., (2004b) Higashijima *et al*., (2004c)
lhx1a	*lim1, lim1a, wu:fe25d04, wu:fj36b06*	ZDB-GENE-980526-347	Toyama & Dawid (1997)
evx1	*cb416*	ZDB-GENE-980526-364	Thaëron *et al*., (2000)
evx2	None	ZDB-GENE-980526-215	Sordino *et al*., (1996)
slc6a5	*glyt2, si:dkey-7n10.12*	ZDB-GENE-050105-2	Higashijima *et al*., (2004b) Higashijima *et al*., (2004c)
gad1b	*gad1, GAD67, gad67*	ZDB-GENE-030909-3	Higashijima *et al*., (2004b) Higashijima *et al*., (2004c)
krt15	*wu:fa91c06, wu:fa95d04, zgc:55334*	ZDB-GENE-040426-2931	Valentin *et al*., (2007)

Table 1. Gene names, previous names, ZFIN identifiers and references for *in situ* hybridization probes used. Column 1 lists genes used in this study. Previous names, where known, are provided in column 2. Column 3 contains the unique ZFIN identification number for each gene. Column 4 provides the reference for the *in situ* hybridization RNA riboprobe used in our experiments.

Table 2

Fig.	Comparison	Gene	Difference between two means	P Value
3C	Uninjected control (73.1 ± 0.9) vs *hmx2;hmx3a* DKD (71.8 ± 1.3)	*hmx3a*	1↓	0.328^
3F	Uninjected control (24.2 ± 0.7) vs *hmx2;hmx3a* DKD (23.1 ± 0.5)	*en1b*	1↓	0.244+
3I	Uninjected control (105.4 ± 1.5) vs *hmx2* SKD (86.8 ± 1.6)	*slc17a6a/b*	19↓	**<0.001**+
3I	Uninjected control (105.4 ± 1.5) vs *hmx3a* SKD (82.8 ± 1.8)	*slc17a6a/b*	23↓	**<0.001**+
3I	Uninjected control (105.4 ± 1.5) vs *hmx2;hmx3a* DKD (70.3 ± 1.3)	*slc17a6a/b*	35↓	**<0.001**+
3I	*hmx2* SKD (86.8 ± 1.6) vs *hmx2;hmx3a* DKD (70.3 ± 1.3)	*slc17a6a/b*	17↓	**<0.001**+
3I	*hmx3a* SKD (82.8 ± 1.8) vs *hmx2;hmx3a* DKD (70.3 ± 1.3)	*slc17a6a/b*	13↓	**<0.001**+
3I	*hmx2* SKD (86.8 ± 1.6) vs *hmx3a* SKD (82.8 ± 1.8)	*slc17a6a/b*	4↓	0.138+
3L	Uninjected control (138.6 ± 2.2) vs *hmx2;hmx3a* DKD (167.5 ± 2.9)	*slc32a1*	29↑	**<0.001**+
3O	Uninjected control (105.4 ± 1.5) vs *hmx2;hmx3a* DKD + *MOR-hmx3a* mRNA (89.2 ± 2.0)	*slc17a6a/b*	16↓	**<0.001**+
3O	*hmx2;hmx3a* DKD (70.3 ± 1.3) vs *hmx2;hmx3a* DKD + *MOR-hmx3a* mRNA (89.2 ± 2.0)	*slc17a6a/b*	19↑	**<0.001**+
NS	WT (105.5 ± 2.2) vs *hmx2*^{SU37} (103.3 ± 0.7)	*slc17a6a/b*	2↓	0.5821^
NS	WT (102.8 ± 0.9) vs *hmx2*^{SU38} (103.6 ± 1.8)	*slc17a6a/b*	2↓	0.700+
5S	WT (88.3 ± 2.9) vs *hmx2*^{SU39} (86.8 ± 4.9)	*slc17a6a/b*	2↓	0.821+
5T	WT (106.0 ± 1.2) vs *hmx3a*^{SU42} (112.0 ± 5.9)	*slc17a6a/b*	6↑	0.389§
5U	WT (102.2 ± 1.1) vs *hmx3a*^{sa23054} (101.0 ± 1.7)	*slc17a6a/b*	1↓	0.567+
NS	WT (97.0 ± 1.2) vs *hmx3a*^{SU43} (85.2 ± 1.2)	*slc17a6a/b*	12↓	**0.019**^
5V	WT (99.8 ± 1.9) vs *hmx3a*^{SU3} (86.4 ± 0.8)	*slc17a6a/b*	13↓	**<0.001**+
5W	WT (102.2 ± 1.9) vs *hmx2;hmx3a*^{SU44} (89.0 ± 1.9)	*slc17a6a/b*	13↓	**0.001**+
5V&W	*hmx3a*^{SU3} (86.4 ± 0.8) vs *hmx2;hmx3a*^{SU44} (89.0 ± 1.9)	*slc17a6a/b*	3↑	0.243+
NS	*hmx3a*^{SU43} (85.2 ± 1.2) vs *hmx2;hmx3a*^{SU44} (89.0 ± 1.9)	*slc17a6a/b*	4↑	0.126+
6K	WT (69.6 ± 0.7) vs *hmx3a*^{SU3} (70.2 ± 0.9)	*hmx3a*	1↑	0.613+
6L	WT (47.6 ± 2.0) vs *hmx3a*^{SU3} (45.0 ± 1.7)	*en1b*	3↓	0.356+
6M	WT (147.4 ± 1.6) vs *hmx3a*^{SU3} (163.0 ± 3.4)	*slc32a1*	16↑	**0.011**^
6N	WT (111.8 ± 3.9) vs *hmx2;hmx3a*^{SU44} (118.3 ± 3.0)	*slc6a5*	6↑	0.237+
6O	WT (61.7 ± 6.1) vs *hmx2;hmx3a*^{SU44} (83.5 ± 2.8)	*gad1b**	22↑	**<0.001**+
6V	WT (150.4 ± 3.4) vs *hmx3a*^{SU3} (173.9 ± 5.2)	*gad1b* (48h)*	24↑	**<0.001**+
6W	WT (143.5 ± 6.7) vs *hmx2;hmx3a*^{SU44} (170.2 ± 8.5)	*gad1b* (48h)*	27↑	**0.024**+
NS	WT (134.9 ± 2.1) vs *hmx2*^{SU39} (133.4 ± 2.9)	*gad1b* (48h)*	1↓	0.685+
6V&W	*hmx3a*^{SU3} (173.9 ± 5.2) vs *hmx2;hmx3a*^{SU44} (170.2 ± 8.5)	*gad1b* (48h)*	3↓	0.704+

Table 2. Statistical comparisons of numbers of cells expressing particular genes.

Statistical comparisons between un-injected control or WT embryos and knockdown or mutant embryos. First column indicates the figure panel that contains the relevant bar chart for the comparison. NS = not shown in a figure. Second column states the genotypes being compared. Numbers within parentheses indicate mean numbers

of cells ± S.E.M. For all cases, cells were counted in all dorsal-ventral spinal cord rows. All of the experiments were conducted on 27 h embryos excepts those indicated with (48h) next to the gene name, which used 48 h embryos. Column three lists the gene that the cell counts, and statistical comparison refer to. Asterisks indicate experiments performed with dextran sulphate (see materials and methods). The fourth column indicates the difference between the two mean values for the embryos being compared. ↑ = increase, ↓ = decrease, NA = Not applicable. Last column shows the P value for the comparison, rounded up to three decimal places. Statistically significant ($P<0.05$) values are indicated in bold. Statistical test used is indicated by superscript symbol: Wilcoxon test (Mann-Whitney, $^{\wedge}$), type 2 Student's t-test ($^{+}$) or type 3 Student's t-test (§). For a discussion of why particular tests were used, see materials and methods.

Table 3.

Mutant allele	**P value for Otolith fusion phenotype**	**P value for survival**
SU35	N/A	0.234
SU36	N/A	0.250
SU37	N/A	0.258
SU38	N/A	0.214
SU39	N/A	0.289
sa23054	<0.001	0.428
SU42	N/A	0.388
SU3	0.850	N/A
SU43	0.391	N/A
SU44	0.752	N/A
SU45	0.126	N/A

Table 3. Statistical analyses of whether the frequencies of homozygous mutants that survive to adulthood or have otolith fusion phenotypes are Mendelian.

First column indicates the mutant allele. These are listed in the same order as in Fig. 4. Second column lists the P value, rounded up to 3 decimal places, for a Chi squared test of the hypothesis that the frequency of embryos with fused otoliths is Mendelian (25%). The third column lists the P value, rounded up to 3 decimal places, for a Chi squared test of the hypothesis that the frequency of mutant embryos that survive to adulthood is Mendelian (25%). Percentages of embryos in these categories and n values are provided in Fig. 4. N/A = not applicable. These are cases where no homozygous mutants survived or had otolith fusion phenotypes.

Table 4.

Allele combination	otolith fusion	# embryos analyzed	P value		Stalled lateral line progression	# embryos analyzed	P value	% strong phenotype	% weaker phenotype
SU39 x SU44	0.007%	268	**<0.001**		0.00%	38	**<0.001**	0.0%	0.0%
SU3 x SU43	22.6%	623	0.165		32.4%	37	0.250	32.4%	0.0%
SU3 x SU44	26.8%	276	0.487		19.4%	36	0.441	19.4%	0.0%
SU43 x SU44	28.3%	279	0.214		31.8%	44	0.296	22.7%	9.1%
sa23054 x SU44	22.4%	303	0.289		26.3%	38	0.703	18.4%	7.9%
sa23054 x SU3	26.6%	139	0.696		17.6%	34	0.244	0.0%	17.6%
SU42 x SU44	22.1%	208	0.337		18.9%	37	0.703	0.0%	18.9%
SU3 x SU42	12.72%	558	**<0.001**		23.3%	192	0.614	2.1%	21.2%

Table 4: Trans-heterozygous mutant analyses identify an allelic series of *hmx3a* mutants.

Parents heterozygous for different mutant alleles were mated and otolith and lateral line progression phenotypes were assayed in their progeny. Otolith phenotypes were assayed at 3 dpf by visual inspection down a stereomicroscope. Lateral line phenotypes were assayed by *in situ* hybridization for *krt15* at 27h. Column one indicates the allele combination tested. Column two shows the percentage of embryos that had fused otoliths and column three shows the total number of embryos analyzed. A chi squared test was performed to test if the frequency of embryos with otolith fusion phenotypes was mendelian and the P value for this test is provided in column 4. Similar experiments were performed to analyze lateral line progression. Column five indicates the percentage of embryos with stalled lateral line progression and column six shows the total number of embryos analyzed. A chi squared test was performed to test if the frequency of embryos with abnormal phenotypes was mendelian and the P value for this test is provided in column seven. In contrast to incrosses of $hmx3a^{SU3}$ or $hmx3a^{SU43}$, where mutant embryos lack any migration of the lateral line primordium into the trunk, in some of these trans-heterozygous crosses, we observed embryos where the lateral line primordium had migrated slightly more caudally. Therefore, we also provide a breakdown in the last two columns of the percentage of embryos that have the $hmx3a^{SU}$ homozygous mutant phenotype (strong phenotype, column eight) vs this slightly weaker phenotype (column nine).

Table 5

Genotype **Embryo Class**	**WT**	**Het**	***hmx3a*^{SU42}** **mutants**	**N value**	**P value**
Uninjected Control	23%	52%	25%	40	0.93
WT-like	31%	31%	38%	16	0.30
Morphant-Like	21%	56%	23%	39	0.61

Genotype **Embryo Class**	**WT**	***hmx3a*^{SU42} mutants**	**P value**
Uninjected Control	117.56 ± 2.26	116.10 ± 1.38	0.5804^{+}
WT-like	116.80 ± 2.89	114.67 ± 2.69	0.6028^{+}
Morphant-Like	86.38 ± 2.15	88.22 ± 5.07	0.7435§
All injected	98.08 ± 4.58	98.80 ± 4.67	0.9134^{+}

Table 5. The lack of spinal cord phenotypes in *hmx3a*^{SU42} mutants is not due to genetic compensation

Spinal cord phenotypes were assessed by *slc17a6a/b in situ* hybridization. *hmx3a* morpholino-injected embryos from a cross of *hmx3a*$^{SU42/+}$ parents were visually inspected on a stereomicroscope and categorized as resembling either a "WT-like" or "morphant-like" spinal cord phenotype. Embryos were genotyped to identify homozygous WTs and mutants. The number of glutamatergic cells in the spinal cord region adjacent to somites 6-10 was then counted in each embryo, using a compound microscope, while blind to genotype. Values in columns 2 and 3 of the lower table indicate the mean number cells ± sem. The P value in the upper table is from a Chi-squared test to determine if the frequencies of different genotypes were mendelian. The P value in the bottom table is either from a type 2 ($^{+}$, performed when data was normally distributed and variances were equal), or type 3 Student's t-test (§, performed when data was normally distributed and variances were unequal) for the comparison of homozygous WT embryos to homozygous *hmx3a*^{SU42} mutants for a particular classification (values on same row). See materials and methods for more information on statistical tests. Statistically significant values are indicated in bold.

Table 6

Genotype **Embryo Class**	**WT**	**Het**	***hmx3a*^{SU3}** **mutants**	**N value**	**P value**
Uninjected Control	20%	55%	25%	44	0.76
Weaker phenotype	20%	56%	24%	41	0.74
Morphant-Like	22%	55%	23%	83	0.54

Genotype **Embryo Class**	**WT**	***hmx3a*^{SU3} mutants**	**P value**
Uninjected Control	106 ± 2.44	94.5 ± 2.62	**0.0062**$^{+}$
Weaker phenotype	102.75 ± 2.27	96.8 ± 1.77	0.0516^{+}
Morphant-Like	70.22 ± 3.76	74.0 ± 2.75	0.7150$^{\wedge}$
All injected	80.23 ± 4.01	81.86 ± 2.78	0.7353^{+}

Table 6. The incomplete penetrance of the spinal cord phenotype in *hmx3a*^{SU3} mutants is not due to genetic compensation

Spinal cord phenotypes were assessed by *slc17a6a/b in situ* hybridization. *hmx3a* morpholino-injected embryos from a cross of *hmx3a*$^{SU3/+}$ parents were visually inspected on a stereomicroscope and categorized as resembling either a "weaker" or more severe, "morphant-like" spinal cord phenotype. Embryos were genotyped to identify homozygous WTs and mutants. The number of glutamatergic cells in the spinal cord region adjacent to somites 6-10 was then counted in each embryo, using a compound microscope, while blind to genotype. Values in columns 2 and 3 of the lower table indicate the mean number cells ± sem. The P value in the upper table is from a Chi-squared test to determine if the frequencies of different genotypes were mendelian. The P value in the bottom table is either from a Wilcoxon test (Mann-Whitney, $^{\wedge}$, performed when data was not normally distributed) or from a type 2 Student's t-test ($^{+}$, performed when data was normally distributed and variances were equal) for the comparison of homozygous WT embryos to homozygous *hmx3a*^{SU3} mutants for a particular classification (values on same row). See materials and methods for more information on statistical tests. Statistically significant values are indicated in bold.

Table 7.

SU Allele	Gene(s)	sgRNA(s) Sequence(s)	F0 Screening		Stable Mutant Screening	
			Method(s)	**Primer Sequences**	**Method(s)**	**Primer Sequences**
35	*hmx2*	GGTATGGATGGTGTCAAATG	HRMA	FW: TGTTTGTGTGTCGCATTGGTG RV: TGTCTTCAGAAACGGGAGACAT	Sequencing	FW: CAACAGTCGATCAAACAGTCAGAG RV: GTGGACTCGAGTTGATAAACCTG
36	*hmx2*	GGTATGGATGGTGTCAAATG	HRMA	FW: TGTTTGTGTGTCGCATTGGTG RV: TGTCTTCAGAAACGGGAGACAT	HRMA	FW: TGTTTGTGTGTCGCATTGGTG RV: TGTCTTCAGAAACGGGAGACAT
37	*hmx2*	GGTATGGATGGTGTCAAATG	HRMA	FW: TGTTTGTGTGTCGCATTGGTG RV: TGTCTTCAGAAACGGGAGACAT	PCR	FW: CAACAGTCGATCAAACAGTCAGAG RV: GTGGACTCGAGTTGATAAACCTG
38	*hmx2*	5': GGTATGGATGGTGTCAAATG 3': GGTTCCAGGATAATACAGTG	PCR	FW: TCAACAGTCGATCAAACAGTCAG RV: GAACCGTGTTGCTTTTGTGTTTTAC	PCR	FW: TCAACAGTCGATCAAACAGTCAG RV: GAACCGTGTTGCTTTTGTGTTTTAC
39	*hmx2*	5': GGACCGGACTCCGTCGTTTG 3': GGTTCCAGGATAATACAGTG	Nested PCR	Nested 1 FW: GCAAATGAGGGCACGTTTCAC RV: GGACATATACAGAACCGTGTTGC Nested 2 FW: TGAATAATTCGGAGGACAGCGGAAG RV: CGTAGACTCGTTTAATTGCTGC	Nested PCR (for deletion) and WT amplicon*	Nested 1 FW: GCAAATGAGGGCACGTTTCAC RV: GGACATATACAGAACCGTGTTGC Nested 2 FW: TGAATAATTCGGAGGACAGCGGAAG RV: CGTAGACTCGTTTAATTGCTGC WT Amplicon FW: CAACAGTCGATCAAACAGTCAGAG RV: GTGGACTCGAGTTGATAAACCTG
42	*hmx3a*	GGAATCTCGGTCGGTGCCTG	HRMA	FW: CGAATGCTAATTTGGCCTCTATTACT RV: TTTTGTTGTCGTCTTCATCGTCC	PCR + restriction digest	FW: TGGCAAAGTGACACGACCAG RV: GAGAACACCGTGCGAGTTTTC Restriction enzyme: BanI
3	*hmx3a*	GGAATCTCGGTCGGTGCCTG	HRMA	FW: CGAATGCTAATTTGGCCTCTATTACT RV: TTTTGTTGTCGTCTTCATCGTCC	PCR	FW: TGGCAAAGTGACACGACCAG RV: GAGAACACCGTGCGAGTTTTC
43	*hmx3a*	GGAATCTCGGTCGGTGCCTG	Fluorescence and/or PCR	FW: GAGAACACCGTGCGAGTTTTC RV: AGTTTCCTGGCAGCATATCCAG	Fluorescence and/or PCR and WT amplicon*	PCR FW: GAGAACACCGTGCGAGTTTTC RV: AGTTTCCTGGCAGCATATCCAG WT Amplicon FW: TGGCAAAGTGACACGACCAG RV: GAGAACACCGTGCGAGTTTTC
44	*hmx2; hmx3a*	5: GGGGCACGTACAATAGCAAA 3': GGTTCCAGGATAATACAGTG	Nested PCR	Nested 1: FW: GTTAGACTTTGCAATGCTCGTG RV: GGACATATACAGAACCGTGTTGC Nested 2: FW: CCTTTTTGCTATTGCCTTCATC RV: CGTAGACTCGTTTAATTGCTGC	Nested PCR (for deletion) and WT amplicon*	Nested 1: FW: GTTAGACTTTGCAATGCTCGTG RV: GGACATATACAGAACCGTGTTGC Nested 2: FW: CCTTTTTGCTATTGCCTTCATC RV: CGTAGACTCGTTTAATTGCTGC WT Amplicon FW: TGGCAAAGTGACACGACCAG RV: GAGAACACCGTGCGAGTTTTC

SU Allele	Gene(s)	sgRNA(s) Sequence(s)	F0 Screening		Stable Mutant Screening	
			Method(s)	Primer Sequences	Method(s)	Primer Sequences
45	*hmx2; hmx3a*	5: GGGGCACGTACAATAGCAAA 3': GGTTCCAGGATAATACAGTG	Nested PCR	Nested 1: FW: GTTAGACTTTGCAATGCTCGTG RV: GGACATATACAGAACCGTGTTGC Nested 2: FW: CCTTTTTGCTATTGCCTTCATC RV: CGTAGACTCGTTTAATTGCTGC	Nested PCR (for deletion) and WT amplicon*	Nested 1: FW: GTTAGACTTTGCAATGCTCGTG RV: GGACATATACAGAACCGTGTTGC Nested 2: FW: CCTTTTTGCTATTGCCTTCATC RV: CGTAGACTCGTTTAATTGCTGC WT Amplicon FW: TGGCAAAGTGACACGACCAG RV: GAGAACACCGTGCGAGTTTTC

Table 7. sgRNA and primer sequences used for *hmx*2, *hmx3a* and *hmx2;hmx3a* CRISPR mutagenesis.
Column 1 lists SU allele designation. Column 2 provides the name of the targeted gene or genes. Columns 3 and 4 indicate the method and primer sequences used to screen founder fish (HRMA = high resolution melt analysis). Columns 5 and 6 indicate the method and primer sequences used to screen stable mutant fish. *In the case of large deletion alleles (where the WT PCR product would be too large to detect by standard PCR conditions) a second PCR (a WT amplicon PCR) is performed. The genomic region targeted by this allele is only present in WT and heterozygous animals that still retain at least one WT copy of the gene. This genomic region is deleted on both chromosomes in homozygous mutant animals. For experimental conditions, see materials and methods.

Figure Legends

Figure 1. Expression of *hmx* genes in WT zebrafish embryos.

Lateral views of *hmx* expression in spinal cord (**A-Y**), hindbrain (**N', S', X'**), eye and ear (**A', E', F', J', K', O', P', T', U', Y'**) and lateral line primordium and neuromasts (**B-C, G-H, L-M, Q-R**) at 19 h (**A-E, A', E'**), 24 h (**D'**), 27 h (**F-J, F', J'**), 36 h (**K-O, K', O'**), 42 h (**P-T, P', Q'**) and 48 h (**U-Y, U', Y'**). Rostral, left; Dorsal, up. (**B-C, G-H, L-M, Q-R, V-W**) *hmx2* and *hmx3a* are expressed in spinal cord, lateral line primordium (white asterisks), neuromasts (black asterisks), and anterior ear (data not shown) at all stages examined, although *hmx2* spinal cord expression initially appears weaker than *hmx3a* and does not extend as far caudally. (**A, A', E, E', F, F', J, J', K, K', O, O', P, P', T, T', U, U', Y, Y'**) *hmx1* and *hmx4* are not expressed in spinal cord at any of these stages but are expressed in the eye (black arrowheads) and posterior-ventral ear and adjacent ganglion of the anterior lateral line (white arrowheads). (**D, I, N, N', S, S', X, X'**) *hmx3b* is not expressed in WT spinal cord at any of these stages. The only expression we observed was in the hindbrain between 36 and 48 h (arrows). (**D'**) *hmx3b* is also not expressed in *mib*^{ta52b} mutants. Inset shows spinal cord but there is no expression in any other tissue either. (**F', J', K', N', O', P', S', T', U', X', Y'**). The background (diffuse, non-specific staining) in these pictures is higher because we exposed the embryos to prolonged staining to ensure that there was no weak spinal cord expression, and the large ventricles of the hindbrain can trap anti-sense riboprobes. Scale Bar = 50 µm (**A-Y**), 120 µm (**A', E', F', J', K', N', O', P', S', T', U', X', Y'**).

Figure 2. *hmx2* and *hmx3a* are expressed in V1 and dI1 interneurons.

(**A**) Schematic showing neurotransmitter and post-mitotic transcription factor phenotypes of the spinal interneurons found in the dorsal-ventral spinal cord region shown in panels C-H. It is currently unclear whether V0v interneurons express Lhx1/5 (*). (**B**) Heatmap analysis of gene expression profiling of V1 interneurons. A three-class ANOVA analysis of differential expression was performed on different FAC-sorted populations of cells. Class 1: All post-mitotic spinal neurons. Class 2: V1 interneurons. Class 3: All trunk cells. Each column is a different biological replicate. Rows show relative expression levels for a single TF as normalized data transformed to a mean of 0, with standard deviation of +1 (highly expressed) or -1 (weakly/not expressed) sigma units. Adjusted P values, corrected for multiple testing are <0.000001 for all genes shown. For more information on these experiments see (Cerda et al., 2009). Expression profiles are included for positive control genes (green) *en1b* and *pax2a* that are expressed by V1 cells and negative control genes (purple) *gata3* and *vsx1* that are expressed by other spinal cord interneurons but not V1 cells. Data for *lhx1a, lhx5* and *hmx3a* shows that they are co-expressed in V1 interneurons. (**C-H**) Lateral views of spinal cord at 27 h. Rostral, left; Dorsal, up. *hmx2* and *hmx3a* are co-expressed (**C**) in V1 and dI2 interneurons. (**D-H**) V1 interneurons are inhibitory (**D**) and express *en1b* (**E**). dI2 interneurons are glutamatergic (excitatory) (**F**) and express *lhx1a* (**G**) but not *evx1* (**H**). Asterisks = double-labeled and white crosses = single-labeled *hmx3a*-expressing cells (green). Expression of other genes is red. Scale bar = 20 µm.

Figure 3. *hmx2/3a* double knockdown (DKD) embryos have fewer excitatory (glutamatergic) and more inhibitory spinal interneurons.

(**A-B, D-E, G-H, J-K, M-N**) Lateral views of spinal cord at 27 h. Rostral, left; Dorsal, up. (**C, F, I, L, O**) Mean number of cells expressing specific genes in a precisely-defined spinal cord region adjacent to somites 6-10 at 27 h. All counts are an average of at least 5 embryos. All counts are of cells on both sides of the spinal cord except for *en1b* (F) which are for just one side of the spinal cord. Error bars indicate SEM. Statistically significant ($p < 0.001$) comparisons are indicated with brackets and three asterisks. All data were first analyzed for normality using the Shapiro-Wilk test. Data set in **C** is non-normally distributed and was, therefore, analyzed with the Wilcoxon (Mann-Whitney) test. Data sets in **F, I, L, O** are normally distributed and so the F test for equal variances was performed. Each pairwise combination of data sets has equal variances and so a type 2 (for equal variances) student's t-test was performed. Mean numbers of cells and P-values are provided in Table 2. (**A-F**) There is no change in the number of *hmx3a*- or *en1b*-expressing spinal cells in *hmx2/3a* DKD compared to un-injected control embryos, suggesting that V1 and dI2 interneurons do not die or transfate/change into different cell types. (**G-I**) The number of *slc17a6a/b*-expressing (excitatory) spinal cells is reduced in both double and single knockdown (SKD) embryos, with the reduction being more severe in DKD embryos. (**J-L**) Concomitantly, there is a statistically significant increase in the number of *slc32a1*-expressing (inhibitory) cells in DKD embryos. (**M-O**) Injection of a morpholino-resistant *hmx3a* mRNA partially rescues the number of spinal excitatory cells in DKD embryos. Scale bar = 30 µm.

Figure 4. Summary of *hmx2/3a* mutant alleles analyzed and their phenotypes when homozygous.

Left-hand side: schematics of 11 mutant alleles analyzed in detail. Top row = genomic locus; lower rows indicate predicted protein products. There is a 6455 bp gap between *hmx2* and *hmx3a*. Right-hand side: Column 1: frequency of embryos with otolith fusion phenotypes from incrosses of heterozygous (z) or homozygous (mz) parents. n = total number of embryos examined (Fig. 5 and data not shown). Column 2 indicates whether a reduction in the number of spinal excitatory cells was observed at 27 h in homozygous mutants, as assayed by *in situ* hybridization for the expression of *slc17a6a/b* (Fig. 5 and data not shown). Column 3: Frequency of viable adult homozygous mutants. n = total number of adult fish genotyped from crosses of heterozygous parents. In all cases where adult homozygous mutants were identified, the numbers of these fish are not statistically significantly different from expected mendelian ratios, as assayed by a Chi Squared test. In all cases P> 0.214. P values are provided in Table 3. All *hmx2* mutant alleles recovered to date are homozygous viable and homozygous mutants do not have a reduction in the number of glutamatergic spinal interneurons or otolith fusions. This is the case, even for embryos from incrosses of fish homozygous mutant for the most severely deleted *hmx2* alleles ($hmx2^{SU38}$ and $hmx2^{SU39}$). $hmx3a^{sa23054}$ mutants are also homozygous viable. They have variable, incompletely penetrant otolith fusion phenotypes. Strikingly, only 27.41% of embryos from an incross of homozygous mutants parents

have otolith fusion phenotypes. *hmx3a*^{sa23054} mutants do not have a reduction in the number of glutamatergic spinal interneurons. *hmx3a*^{SU42} mutants are homozygous viable and do not have any obvious phenotypes, even though this allele should encode a protein with the same number of WT amino acids as *hmx3a*^{SU43} and only one more WT amino acid than *hmx3a*^{SU3}. *hmx2;hmx3a*^{SU44} and *hmx2;hmx3a*^{SU45} differ only in the amount of upstream sequence that is deleted and have identical phenotypes, so we use them interchangeably in experiments.

Figure 5. Only some *hmx2/3a* alleles have mutant phenotypes.

(**A-R, A', E' G'**) Lateral views. Rostral, left; Dorsal, up. (**A-F, A', E'**) Ear phenotypes examined either by *hmx3a* expression at 27 h (**A-C** & **E'**), or live at 4 dpf (**A', D-F**). (**G-L, G'**) Lateral line primordium phenotypes examined either by *hmx3a* expression (**G', H-J**) or live (**G, K-L**) at 27 h. (**M-R**) Expression of *slc17a6a/b* in the spinal cord at 27 h. (**S-W**) Mean number of cells expressing *slc17a6a/b* in a precisely-defined spinal cord region adjacent to somites 6-10 at 27 h. All counts are an average of at least 5 embryos. Error bars indicate SEM. Statistically significant ($p < 0.05$) comparisons are indicated with brackets and asterisks. $p < 0.05$ = *, $p < 0.001$ = ***. All data were first analyzed for normality using the Shapiro-Wilk test. Data set in **W** is non-normally distributed and therefore analyzed with the Wilcoxon (Mann-Whitney) test. Data sets in **S, T, U** and **V** are normally distributed and so the F test for equal variances was performed. A type 2 (for equal variances) student's t-test was performed for data sets in **S, U** and **V** and a type 3 (for non-equal variances) student's t-test was performed for data set in **T**. P-values are provided in Table 2. (**A-C**) *hmx3a* expression in the ear (inside white dotted lines) and in presumptive neuroblasts anterior to the ear (white arrowheads) is unchanged in *hmx2*^{SU39} (**B**) and *hmx3a*^{SU42} (**C**) mutants, compared to wild type (**A**), but is severely reduced in both the presumptive neuroblasts anterior to the ear and the anterior ear (black arrowhead) in *hmx3a*^{SU3} mutants (**E'**). (**A', D-F**) *hmx3a*^{sa23054} mutants show incompletely penetrant, variable otolith fusion phenotypes, ranging from no fusion (like WT ear in **A'**), through incomplete fusion (**D**), to complete fusion, like that observed at full penetrance in *hmx3a*^{SU3} (**E**) and *hmx2;hmx3a*^{SU44} (**F**) mutant embryos. (**G-J, G'**). At 27 h, the tip of the lateral line primordium (black dotted line, **G**) has reached somite 10 (S7 + arrow = somite 7 boundary) in WT embryos (**G, G'**). This rate of migration is unchanged in *hmx2*^{SU39}, *hmx3a*^{SU42} and *hmx3a*^{sa23054} mutant embryos. (**K-L**) In contrast, the lateral line primordium fails to migrate in *hmx3a*^{SU3} (**K**) and *hmx2;hmx3a*^{SU44} (**L**) mutant embryos. Instead, it is stalled adjacent to somites 1-4 (S1 + arrow = somite 1). (**M-W**). There is no change in the number of spinal excitatory neurons in *hmx2*^{SU39} (**N, S**), *hmx3a*^{SU42} (**O, T**) and *hmx3a*^{sa23054} (**P, U**) mutant embryos compared to WT (**M**). In contrast, there is a statistically significant reduction in *hmx3a*^{SU3} (**Q, V**) and *hmx2;hmx3a*^{SU44} (**R, W**) mutant embryos. Scale bar = 30 µm (**A-L**), 50 µm (**M-R**).

Figure 6. Analysis of *hmx3a* single and *hmx2;hmx3a* double mutants.

(**A-K, P-U & X**) Lateral views of *hmx3a* (**A, F**), *en1b* (**B, G**) *slc32a1* (**C, H**) *slc6a5* (**D, I**), *gad1b* (**E,K, P, Q, S, T**) or *krt15* (**R, U, X**) expression in the spinal cord (**A-K, P, Q, S, T**) or lateral line primordium (**R, U, X**) at 27 h (**A-K, R, U, X**) or 48 h (**P, Q, S, T**). Rostral, left; Dorsal, up. (**K-O, V, W**) Mean number of cells expressing

specific inhibitory genes in a precisely-defined spinal cord region adjacent to somites 6-10 at 27 h. All counts are an average of at least 5 embryos, except panel N where n=4. Error bars indicate SEM. Statistically significant ($p < 0.05$) comparisons are indicated with brackets and asterisks. $p < 0.05$ = *, $p < 0.01$ = **, $p < 0.001$ = ***. White bars indicate WT data and black bars the appropriate mutant data as indicated in key under panel X. All data were first analyzed for normality using the Shapiro-Wilk test. Data set in M is non-normally distributed and therefore analyzed with the Wilcoxon (Mann-Whitney) test. Data sets in K, L, N, O, V and W are normally distributed and so the F test for equal variances was performed. All of these had equal variances so a type 2 student's t-test was performed. P-values are provided in Table 2. (**A, B, F, G, K, L**) As in DKD embryos (Fig. 3), dI2 and V1 interneurons do not die, nor do dI2 interneurons transfate/change in to V1 interneurons in *hmx3a*^{SU3} mutant embryos, since the numbers of *hmx3a-* (**A, F** & **K**) and *en1b*-expressing cells (**B, G** & **L**) do not change compared to WT embryos. (**C, H, M**) There is a statistically significant increase in the number of inhibitory, *slc32a1*-expressing cells in *hmx3a*^{SU3} mutants compared to WT embryos. (**D, I, N**) However, the number of *slc6a5*-expressing cells is unchanged between WT and *hmx2;hmx3a*^{SU44} mutants, whereas there is an increase in the number of GABAergic (*gad1b*-positive) in *hmx2;hmx3a*^{SU44} mutants (**E, K, O**), suggesting that the additional inhibitory cells in the mutant embryos are GABAergic and not glycinergic. (**P, Q, S,T, V, W**) There is an equivalent increase in GABAergic (*gad1b*-positive) cells at 48 h in *hmx3a*^{SU3} and *hmx2;hmx3a*^{SU44} mutant embryos. (**R, U, X**). *hmx3a*$^{SU42/+}$*;hmx3a*$^{SU3/+}$ trans-het embryos have two different lateral line primordium progression phenotypes. Scale bar = 50 µm.

Figure 7. Expression of *hmx* genes before the mid-blastula transition and in mutant zebrafish embryos.
(**A-I**) Lateral views of expression in whole embryos at 1.5 h (16-cells, **A-E**) and in the spinal cord (**F-I**) at 27 h. (**A-E**) Animal pole, up. (**F-I**) Rostral, left; Dorsal, up. (**A-E**) None of the *hmx* genes are maternally expressed at 1.5 h. (**F-I**) *hmx3a* mRNA does not exhibit nonsense-mediated decay (NMD) in *hmx3a*^{SU42} (**F**), *hmx3a*^{sa23054} (**G**), *hmx3a*^{SU3} (**H**) or *hmx3a*^{SU43} (**I**) mutant embryos. Although out of focus, migration of the lateral line primordium (asterisk) is unaffected in *hmx3a*^{SU42} mutant embryos (**F)** but is stalled, and hence is not visible, in *hmx3a*^{sa23054} (**G**), *hmx3a*^{SU3} (**H)** and *hmx3a*^{SU43} (**I**) mutant embryos. See also Fig. 5. Scale Bar = 280 µm (**A-E**), 50 µm (**F-I**).

Figure 1

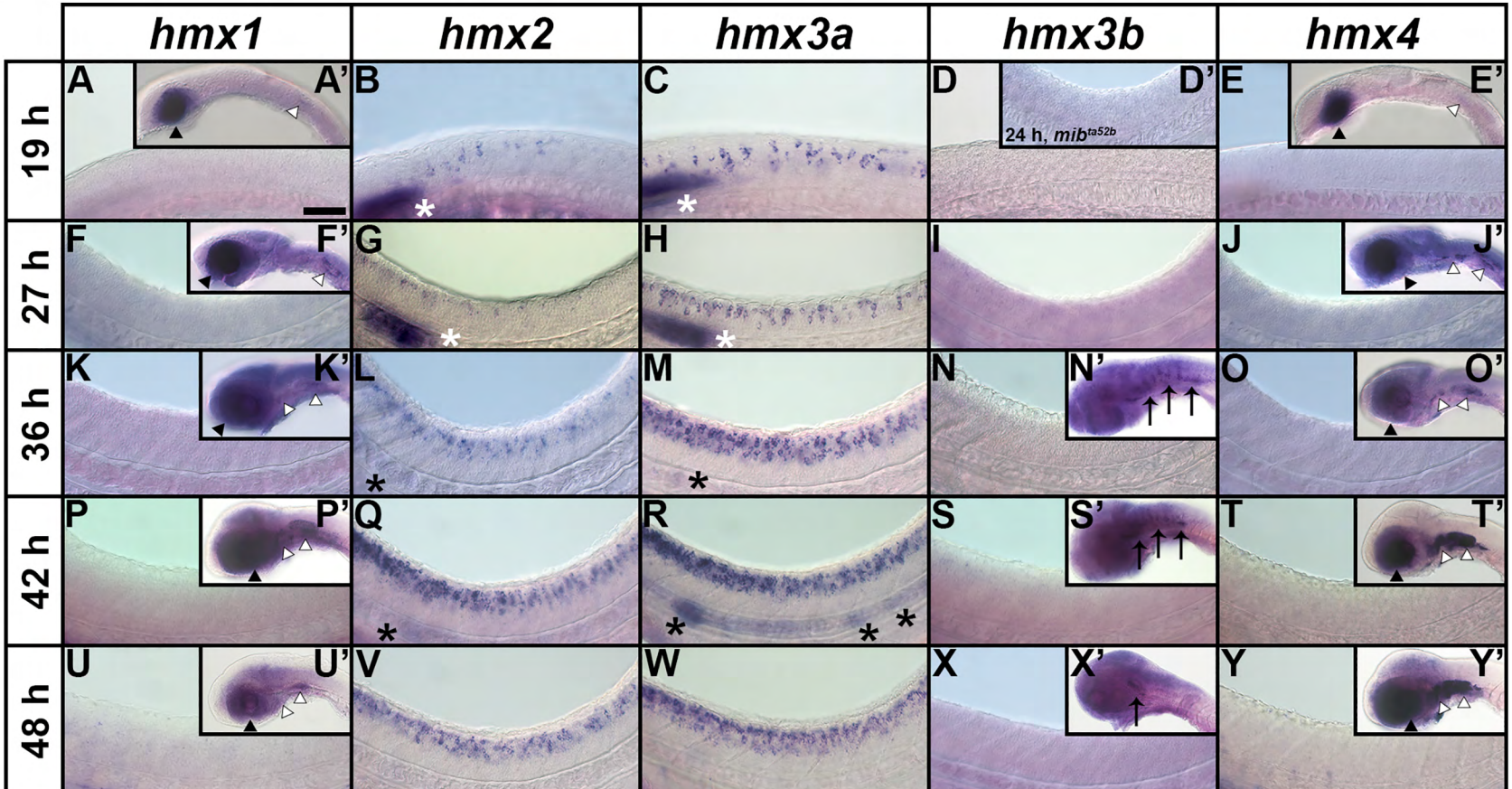
hmx1
hmx2
hmx3a
hmx3b
hmx4
19 h
27 h
36 h
42 h
48 h
A
A'
B
C
D
D'
24 h, mib ta52b
E
E'
F
F'
G
H
I
J
J'
K
K'
L
M
N
N'
O
O'
P
P'
Q
R
S
S'
T
T'
U
U'
V
W
X
X'
Y
Y'

Figure 2

A

Cell Type	Neurotransmitter Phenotype	Post-Mitotic Transcription Factor Phenotype	
dI2	Excitatory		*Lhx1/5*
dI3	Excitatory		
dI4	Inhibitory		*Lhx1/5*
dI5	Excitatory		
dI6	Inhibitory		*Lhx1/5*
V0D	Inhibitory		*Lhx1/5*
V0V	Excitatory	*Evx1/2*	*Lhx1/5**
V1	Inhibitory	*En1b*	*Lhx1/5*

B

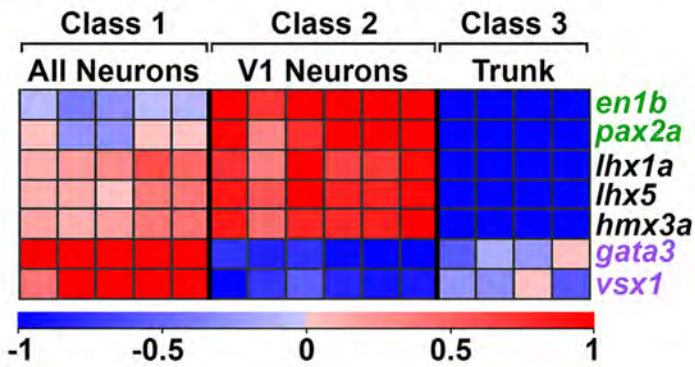

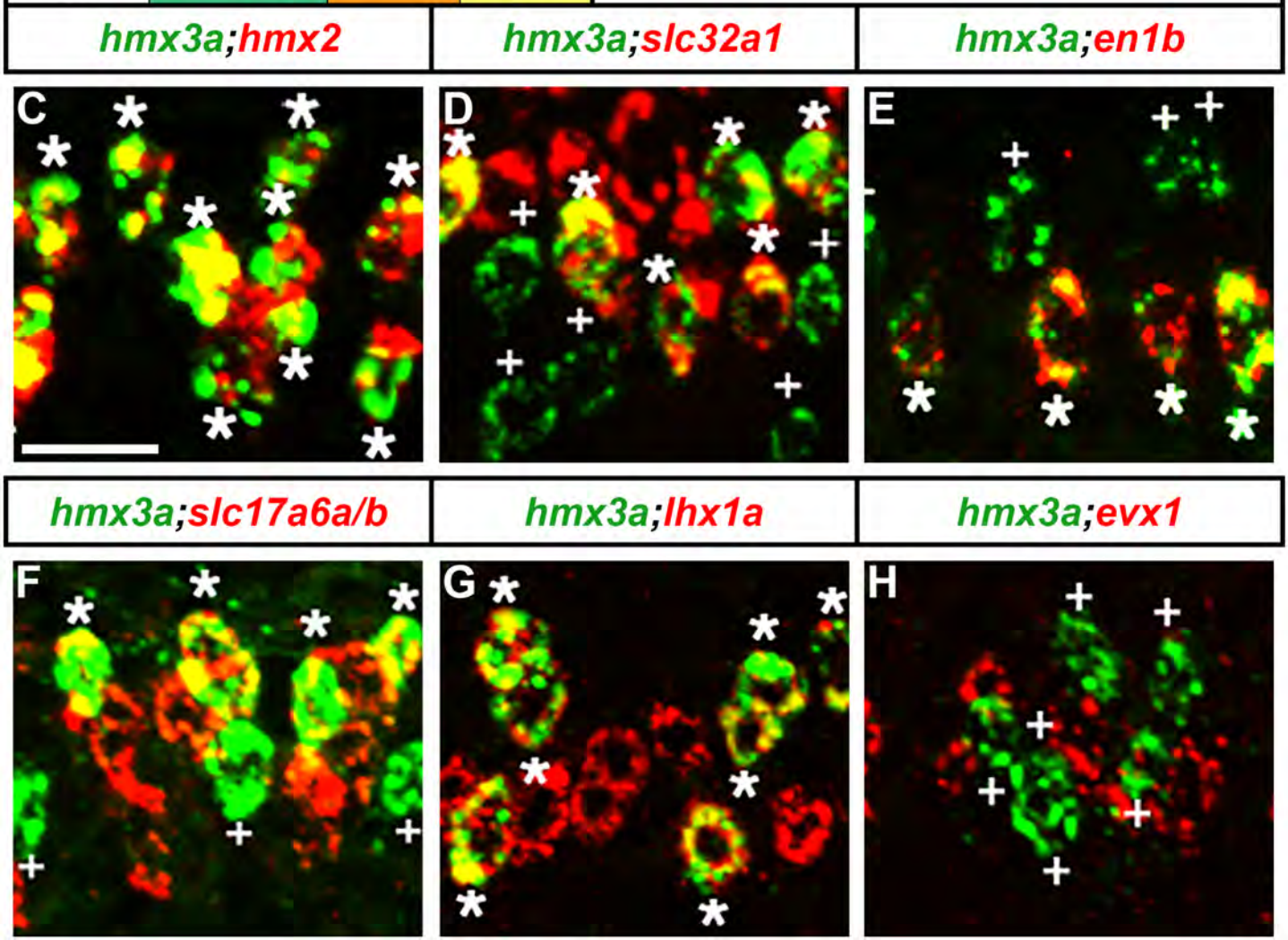

Figure 3

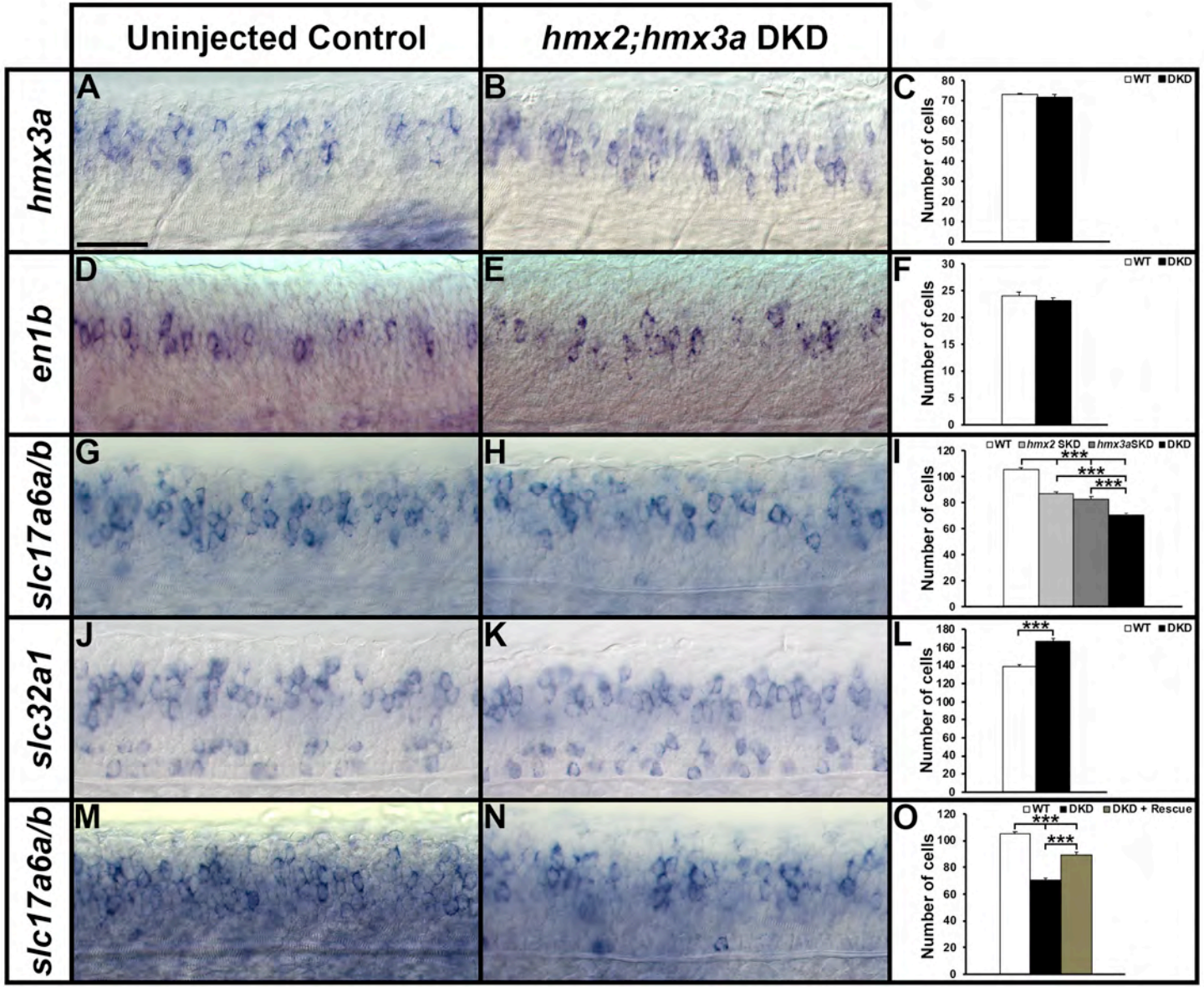
Uninjected Control
hmx2;hmx3a DKD
hmx3a
en1b
slc17a6a/b
slc32a1
slc17a6a/b
A
B
C
D
E
F
G
H
I
J
K
L
M
N
O
WT
DKD
hmx2 SKD
hmx3aSKD
DKD + Rescue
Number of cells
***

Figure 4

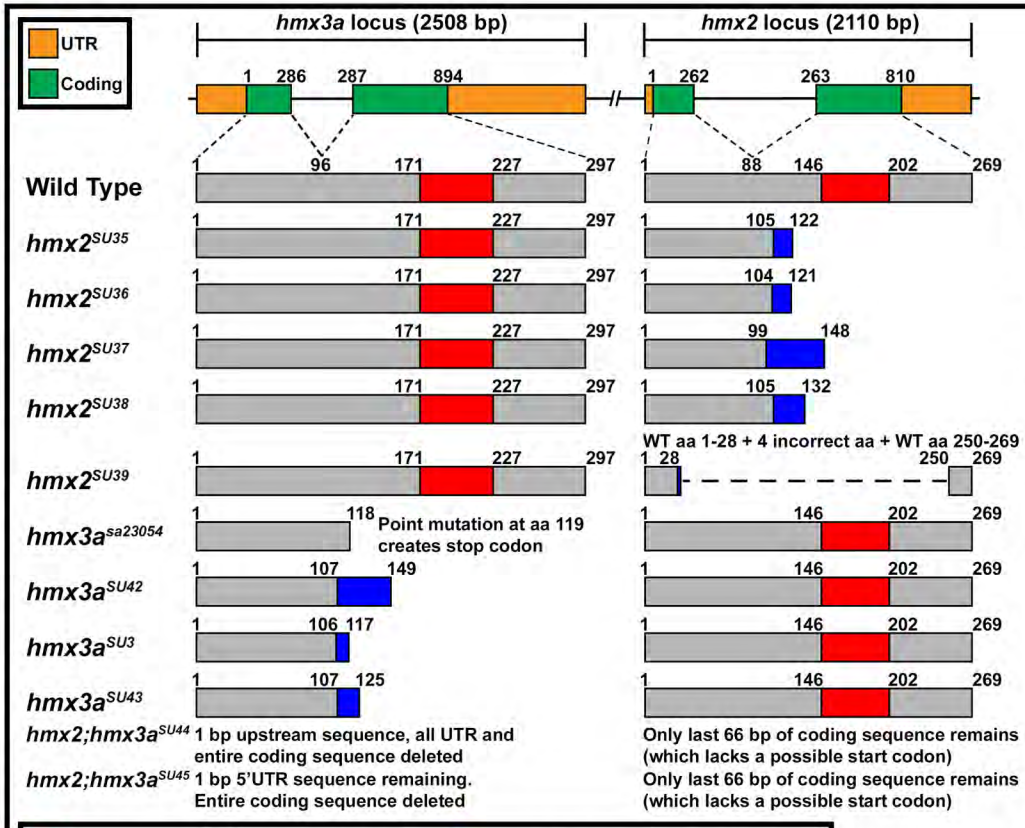

Allele	Fused Otolith Phenotype	dl2 Interneuron Phenotype	Viable Adult Homozygous Mutants
35	0% (n=100; z)	NA	18.03% (n=61)
36	0% (n=100; z)	NA	16.22% (n=37)
37	0% (n=112; z)	NO	20.19% (n=104)
38	0% (n=56; z) 0% (n=77; mz)	NO	33.33% (n=54)
39	0% (n=49; z) 0% (n=228; mz)	NO	30.26% (n=76)
sa23054	12.35% (n=332; z) 27.41% (n=135; mz)	NO	20.78% (n=77)
42	0% (n=121; z)	NO	20.00% (n=65)
3	24.85% (n=2370; z)	YES	NONE
43	23.33% (n=463; z)	YES	NONE
44	25.41% (n=1334; z)	YES	NONE
45	29.52% (n=227; z)	YES	NONE

Figure 5

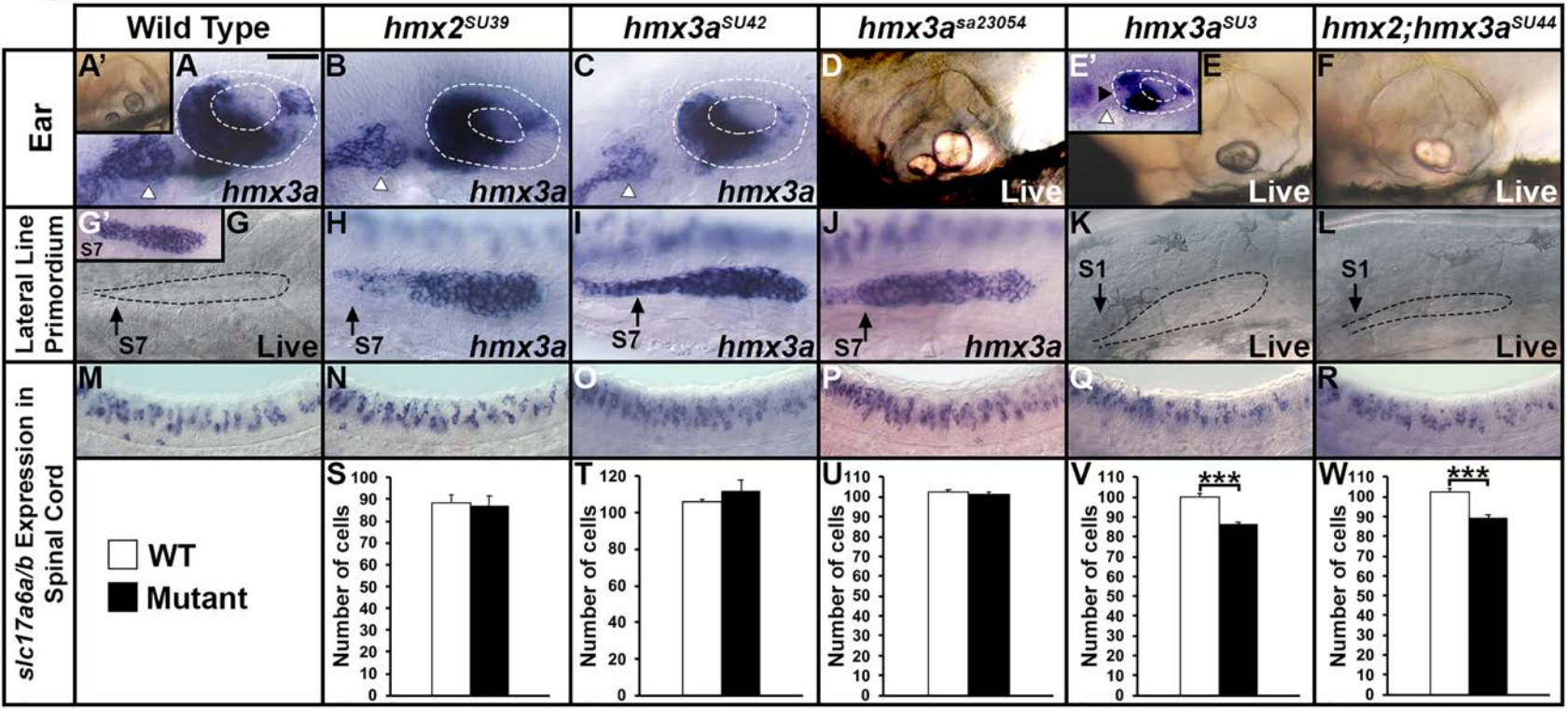
Wild Type
hmx2SU39
hmx3aSU42
hmx3asa23054
hmx3aSU3
hmx2;hmx3aSU44
Ear
Lateral Line Primordium
slc17a6a/b Expression in Spinal Cord
A'
A
B
C
D
E'
E
F
hmx3a
Live
G'
G
H
I
J
K
L
S7
S1
M
N
O
P
Q
R
S
T
U
V
W
WT
Mutant
Number of cells
***

Figure 6

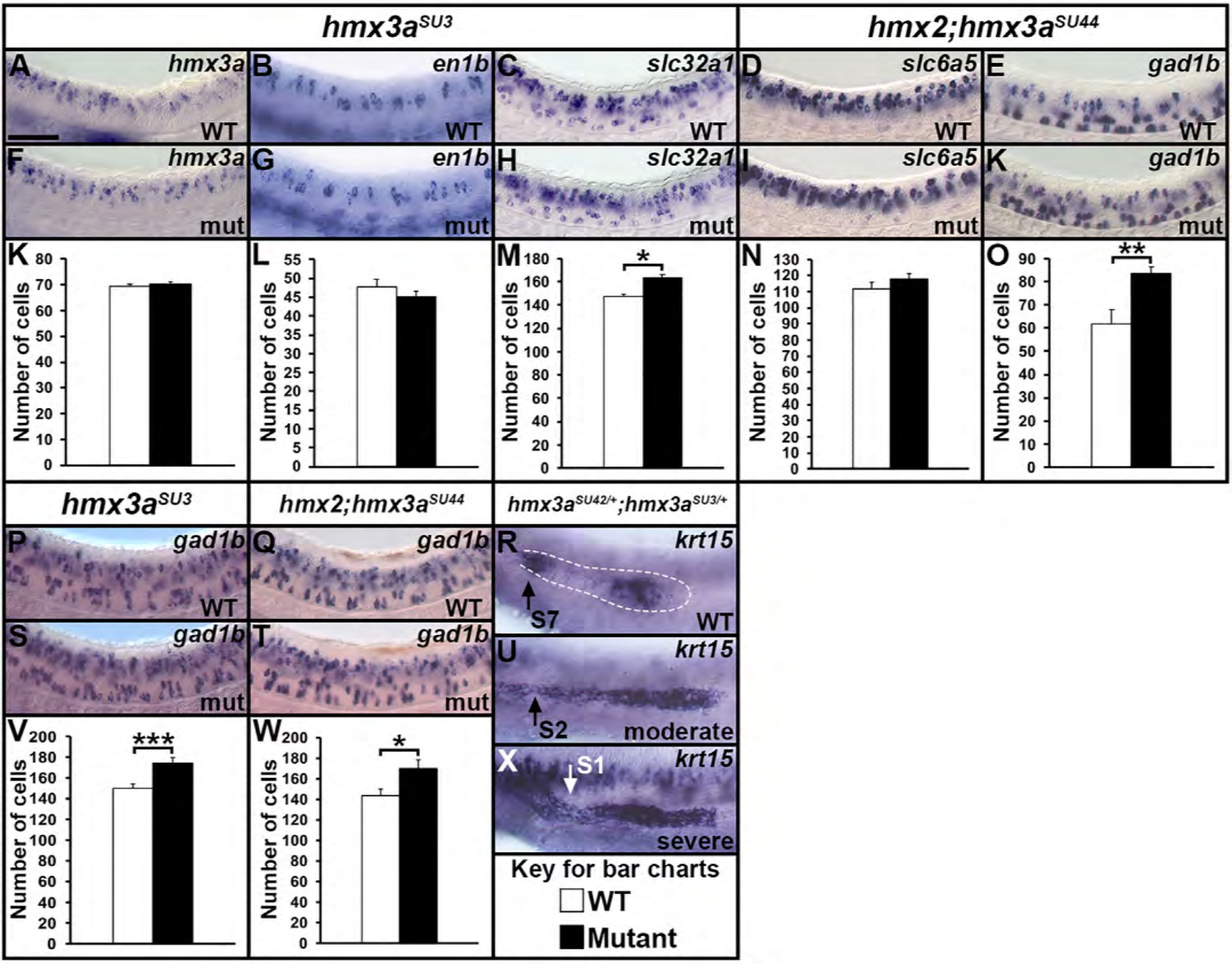
hmx3a^SU3
hmx2;hmx3a^SU44
A hmx3a WT
B en1b WT
C slc32a1 WT
D slc6a5 WT
E gad1b WT
F hmx3a mut
G en1b mut
H slc32a1 mut
I slc6a5 mut
K gad1b mut
K Number of cells
L Number of cells
M Number of cells *
N Number of cells
O Number of cells **
hmx3a^SU3
hmx2;hmx3a^SU44
hmx3a^SU42/+;hmx3a^SU3/+
P gad1b WT
Q gad1b WT
R krt15 S7 WT
S gad1b mut
T gad1b mut
U krt15 S2 moderate
V Number of cells ***
W Number of cells *
X S1 krt15 severe
Key for bar charts
WT
Mutant

Figure 7

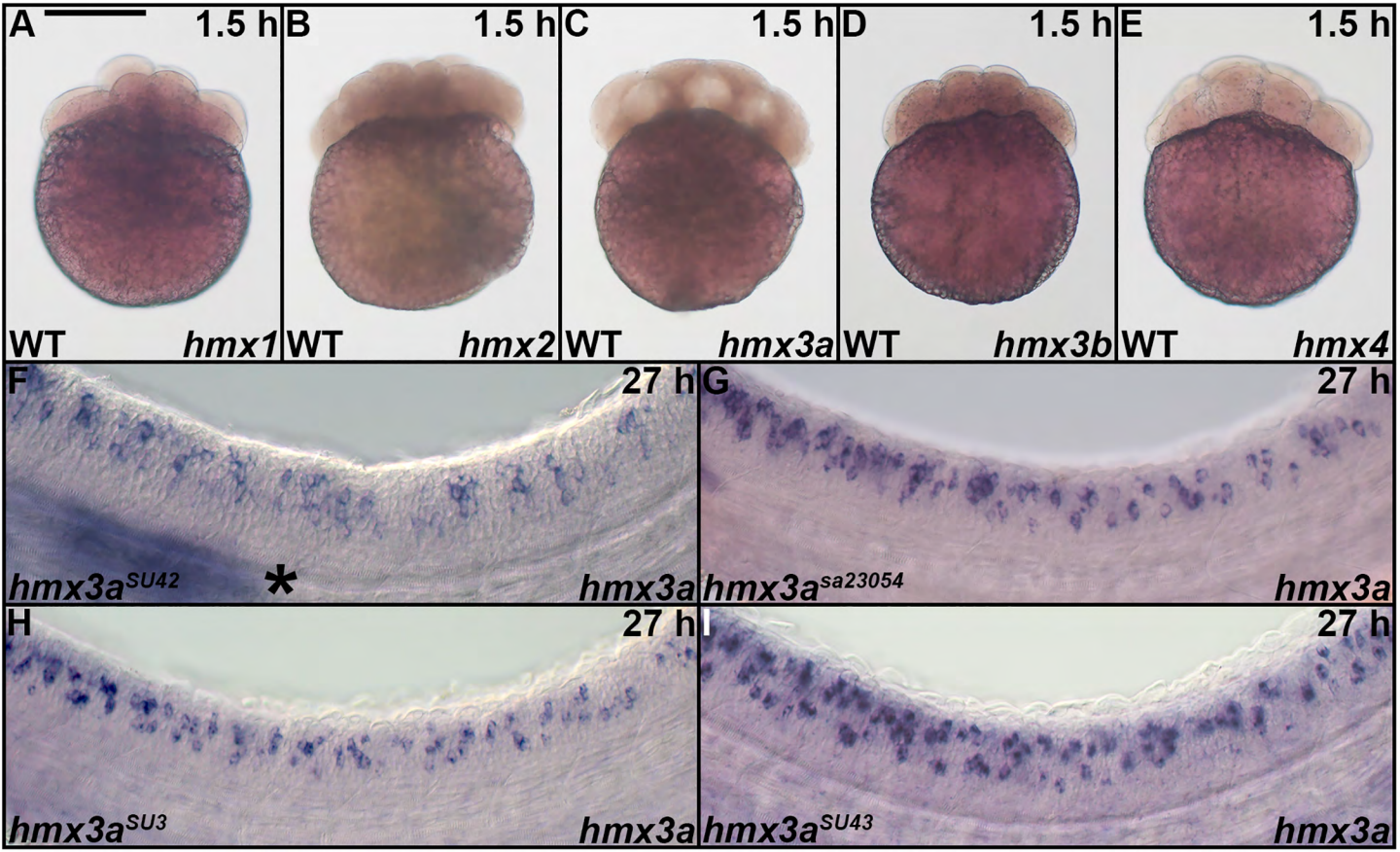
A
1.5 h
WT
hmx1
B
1.5 h
WT
hmx2
C
1.5 h
WT
hmx3a
D
1.5 h
WT
hmx3b
E
1.5 h
WT
hmx4
F
27 h
hmx3a^SU42
*
hmx3a
G
27 h
hmx3a^sa23054
hmx3a
H
27 h
hmx3a^SU3
hmx3a
I
27 h
hmx3a^SU43
hmx3a